University of Texas Rio Grande Valley

ScholarWorks @ UTRGV

8-2021

Force Spun PVDF and TPU Nanofiber Based Triboelectric Nanogenerator for Energy Harvesting and Sensor Application

Sk Shamim Hasan Abir
The University of Texas Rio Grande Valley

Recommended Citation

Abir, Sk Shamim Hasan, "Force Spun PVDF and TPU Nanofiber Based Triboelectric Nanogenerator for Energy Harvesting and Sensor Application" (2021). *Theses and Dissertations*. 800.
https://scholarworks.utrgv.edu/etd/800

FORCE SPUN PVDF AND TPU NANOFIBER BASED TRIBOELECTRIC

NANOGENERATOR FOR ENERGY HARVESTING

AND SENSOR APPLICATION

A Thesis

by

SK SHAMIM HASAN ABIR

Submitted to the Graduate College of
The University of Texas Rio Grande Valley
In partial fulfillment of the requirements for the degree of

MASTER OF SCIENCE IN ENGINEERING

August 2021

Major Subject: Mechanical Engineering

FORCE SPUN PVDF AND TPU NANOFIBER BASED TRIBOELECTRIC

NANOGENERATOR FOR ENERGY HARVESTING

AND SENSOR APPLICATION

A Thesis
by
SK SHAMIM HASAN ABIR

COMMITTEE MEMBERS

Dr. Karen Lozano
Chair of Committee

Dr. M. Jasim Uddin
Committee Member

Dr. Rogelio Benitez
Committee Member

August 2021

ABSTRACT

Abir, Sk Shamim Hasan, <u>Force spun PVDF and TPU nanofiber based triboelectric nanogenerator for energy harvesting and sensor application</u>. Master of Science Engineering (MSE), August 2021, 44 pp., 23 figures; 95 references.

Flexible triboelectric nanogenerator (TENG) is the next generation potential candidate for wearable and portable electronics. In this study, nanofiber based TENG has been demonstrated for energy harvesting and biomechanical sensing applications. The TENG was prepared by force spun polyvinylidene fluoride (PVDF) and gold (Au) sputtered thermoplastic polyurethane (TPU) nanofiber (NF) layers. The experimental characterization of the PVDF-TPU/Au NF-TENG revealed that surface modification by creating extra frictional area of the TPU fiber membrane resulted the maximum open circuit voltage (254 V) and short circuit current (86 μA) output at 240 bpm (beats per minute) load frequency which was respectively 112% and 87% greater than bare PVDF-TPU NFs based TENG with the active contact surface area 1.25×1.0 in^2. Furthermore, the TENG was able to light up 75 LED of 1.5 V each by hand tapping at 240 bpm frequency. The results of the resistive loads and capacitor tests exemplified that our proposed TENG offered a viable prospect for a simple and high performance self-chargeable electronics. Consequently, the possible chest, thigh, forearm, and bicep muscle sensors with different body movement, illustrated the possibility of flexible and cost-effective body motion sensors as well.

DEDICATION

All praise to almighty Allah, without His blessings I won't be able to make it until this point. I want to dedicate this work to my parents, Sk Shamsel Haque and Afroza Banu, who have always showed me their love, and support from my home country; my lovely wife, Jannatul Ferdous, for her encouragements, sacrifice, compassion, mental support, and love; also, my sibling, Sharmin Akther Munia for her love and affection.

ACKNOWLEDGMENTS

TABLE OF CONTENTS

LIST OF FIGURES

CHAPTER I

INTRODUCTION

In order to create a triboelectric nanogenerator, two electrostatic material is essential and selecting this material is very important as the performance the TENG cell depends on the material's inherent polarity difference and charge ejection/acceptation capabilities. For making the TENG cell flexible and stretchable, polymer is the most proper material which serves all the requirements [1], [2]. Though TENG can utilize various modes of available energy however considering cost effectiveness and ease of fabrication we focused on scavenging mechanical energy with contact and separation mode of the TENG. Making high performance TENG serve for long time without damaging the layer, polymeric nanofiber based TENG is a good choice in this consideration. Compare to the polymer film/composite which are often thick and face low quality mechanical stretchability, the nanofibers serve much better as they provide porous morphology and rough surface area to cause friction to generate triboelectric effect [3], [4].

In this study, we have synthesized PVDF nanofiber with by Forcepsinning® technique as negative layer with high affinity toward electron. PVDF has gained lots attention over the years due to its high piezoelectric coefficient and dielectric constants. Besides, continuous and homogeneous PVDF NFs result in β phase over other phases, yields very good electroactive characteristics special high polarizability and dielectric properties which promote significant electrical output of the TENGs [5], [6]

Compare to other positive polymer with good electron ejection capability, TPU has been studied very little in this regard. In this experiments, we have fabricated heterogenous and flexible TPU nanofiber mat as a positive layer by forcespinnig technique as well due to good charge density difference with respect to PVDF [7]. However, bare polymeric nanofiber doesn't high performance triboelectric effect. To overcome this drawback, in this manuscript we have reported for the very first time a very simple and straight forward technique to enhance the conductivity and discharge effect of TPU with coated gold (Au) nanolayer by plasma sputtering technique on the TPU nanofiber surface as gold amplify charge transfer property of a surface while making the nanofiber layer mechanically flexible with high rough surface area with enhanced frictional contact area which is the imperative requirement to boost up the performance of TENG [8]–[11].

The experimental characterization illustrated that the embedded Au layer on the TPU surface resulted high open circuit voltage and short circuit current output in compare to bare PVDF/TPU nanogenerator cell. The nanofiber based triboelectric nanogenerator (NF-TENG) showed a very good potential of charging small electronics within a short period of time and very sensitive and effective biomechanical motion sensor.

CHAPTER II

REVIEW OF LITERATURE

Over the last few years, with the expansion of the flexible and stretchable wearable electronic devices, portable power storage for powering small electronics have seen great deal of attention by the researcher [12]–[15]. However, conventional power source like batteries often face limited life span, heavy weight and not eco-friendly [16], [17]. To resolve these issues, various modes of nanogenerators have been introduced that can convert solar, thermal, mechanical, chemical energy into continuous and maintenance free electricity [18]. These nanogenerators typically utilize following phenomena such as piezoelectricity, pyroelectricity, photoelectricity, electromagnetic effect to harvest [19]–[21]. Though they have shown great prospects till now however they often lack high power output. Another highly energy efficient mechanism is the triboelectric effect that can harness electricity from mechanical energy [18], [22], [23].

In 2012, triboelectricity phenomenon was explored first by Wang et al. for scavenging ambient mechanical energy and since then triboelectric nanogenerator (TENG) has caught great interest among the researchers due to its light weight, easy fabrication, durability, robustness, and cost effectiveness [24]. Currently TENGs are being highly exploited as energy harvesters and self-powered sensors. TENG works based on the principle of the electrification of two layers followed by triboelectric effect [14], [25], [26]., after they get separated from their initial contact

mode. Charges are generated while top and bottom layer of TENG being continuously separated and contacted, results a potential difference between two layers yields into flows of current back and forth in the external circuit to balance the surface potential through electrodes which is already connected to the triboelectric layers. As a result, selecting triboelectric material with good charge generation capability is the main consideration to fabricate a TENG [18], [24]. Polymer has been widely used for making layers of the TENG cell due to its flexibility and free of environmental corrosion [27]. Usually polymer with functional group inclined to eject electron during mechanical bending and stretching used as positive layer while functional group prone to accept electron tend to be negatively charged layer [28].

The performance of nanogenerator depends on the frictional contact area, surface chemical properties, charge density, dielectric properties of the TENG materials. Among versatile materials PVDF [29], polytetrafluoroethylene (PTFE) [30], polydimethylsiloxane (PDMS) [31], polyimide (PI) [25], poly(vinylidene fluoride-trifluoroethylene) (PVDF-TrFE) [32], poly(vinylidene fluoride-co-hexafluoropropene) (PVDF-HFP) [33], polyvinyl chloride (PVC) [34], poly propylene (PP) [35], polyacrylonitrile (PAN) [36] polymers of various forms like thin film, nanofiber, nanocomposite and aerogel [23], [30], [37], [38] have been widely used as negative layer owing to high charge affinity, flexibility, high dipole moment, durability which are very important parameters not only to harness mechanical energy as nanogenerators but also as UV detector [5], antibacterial application [26], air filtration [39], facial respiration [40], biomechanical motion and pressure sensing application [41], [42]. To harness mechanical energies and capitalize this TENGs in wearable electronics and human motion detection application selecting a positive material has similar importance. However, compare to the negative material, tribo positive materials are relatively limited such as aluminum (Al) [43],

copper (Cu) [31], silver (Ag) [44], polymeric materials (e.g., nylon [28], TPU [35], cellulose [45], poly(3-hydroxybutyrate-co-3-hydroxyvalerate) (PHBV) [6], polyvinyl alcohol (PVA) [26]) are commonly used.

Compare to polymer film based triboelectric layer which favors brittleness results absence of mechanical robustness, whereas fiber based TENGs offers more distinctive and inherent advantages like flexibility, breathability, stretchability, and most importantly effective contact surface area [35]. In addition, due to great flexibility and breathability, nanofiber based TENGs can also be used as active sensor to detect mechanical response of human motion [46]–[48]. The main advantage of the TENG sensors is that they can perform without an external power supply [49], [50]. Typically, sensors are employed to detect target signal but this multifunctional TENG can serve both as an energy harvesting device as well as a self-powered sensor [51], [52].

One of the most challenging devices to develop for wearable electronics application. Though fiber based TENG has offered many advantages for highly attractive potential for energy harvesting and medical sensors [53]–[55], there are various modes of making fibrous structure like on various core and shell fiber structure [56], woven and knit fiber structure [46], [57], and membrane like structure [58]. Compare to the other modes, the nonwoven based membranous structure nanofiber mat is the most promising medium for fabricating wearable TENGs. It has been widely studied not only for its good mechanical properties; rather nanofibers based TENG can offer better electrical properties as well [14], [35], [59]–[61]. Moreover, the prime consideration of the wearable electronics is to offer stable but repeated signal with same time interval, nanofiber based TENG offers string potential [13], [33], [55], [62]. Considering the excellent electrical and structural properties of nanofiber based TENG, these can be easily

5

attached to human skin and moreover, can easily distinguish different bending angle of human body parts according to their posture [31], [63], [64].

Currently, nanofiber based TENG layers using electrospinning technique has been applied recently which aid nano to micro scale fiber diameters, smaller porous structure, and large surface area to volume ratio [27], [31], [32]. Electrospinning process uses electrostatic forced to make nanoscale fiber and quite successful in lab scale production. However, this procedure has intrinsic drawback most importantly costly experimental setup and low fiber output. As a consequence, in this study we have used forcespinning technique, a very cost-effective technique to prepare the nanofiber for both triboelectric layer which uses centrifugal force to synthesis nanofiber [65], [66]. Forcespinning method of making fiber favors high production rate 1g/min compare to 0.1 g/hr. in electrospinning results high yield and moreover, output is 600 time greater.

Nevertheless, though there has been noticeable output achieved in TENGs field, the power output is not up to the mark to use it in real-time wearable electronics. So, there is still room to improve further of their performances. Currently, many researchers are trying surface modification to boost up the performance by incorporating various functional groups with different materials such as metal oxides [36], [40], nanoparticles [12], carbonaceous material (e.g., graphene oxide (GO) [6], multiwall carbon nanotube (MWCT) [32], silver nanowires (Ag-NW) [26], MXene materials [28] in TENG material matrix. Though surface modification of these triboelectric layers with different filling materials stated above to improve dielectric constants and high charge density difference between two layers for better output has been emphasized mostly, the methods of introducing these filler material often suffers difficulty due to

required expensive equipment, complicated synthesis procedure as well as agglomeration and precipitations during making of polymer solution to produce fibers [16].

Among various tribo negative polymer nanofiber (NF), PVDF NF was employed in this study due to its lightweight, ease of fabrication, flexibility [14], [28]. Among α, β, γ, δ, and ε phases of the PVDF fiber, the β phase has better polar response with an orthorhombic unit cell crystalline structure [28], [67]. Thus, its dipole orientation along the polymer chain makes it suitable piezo and triboelectric nanogenerator application. This β induced more effectively by stretching the polymer and making fiber out of polymer solution yield better stretch on the polymer morphology [55]. Furthermore, compare to other electro positive polymer, TPU polymer based NF has good mechanical stretchability, and better electron ejection capability [13], [35]. Moreover, due its high rough surface structure, it makes ideal candidate to investigate as a tribo positive layer. Both PVDF and TPU nanofibers in this experiment were synthesized by forcepsinning technique at ambient condition.

Fabricate a TENG with cost effective point of view at the same time increasing the performance by simple techniques has not been studied much. The prepared fiber mat exhibited excellent flexibility and stretchability which is favorable to harvest mechanical energy. To upgrade the TENG performance, later an inexpensive thin layer of gold was coated for further making the surface coarse and rough, eventually resulted more frictional area. This plain and facile technique of improving TENG performance was further utilized to charging electronics, lighting up LED and detecting biomechanical motion.

CHAPTER III

EXPERIMENTAL TECHNIQUES

Forcespinning (FS)

Over the few decades, there has been a noticeable demand for polymeric nanofibers which has been widely used for various applications including tissue engineering [68], drug delivery [69], antibacterial application [70], filtration [71], Li/Na ion battery anodes [72], photoluminescent nanofiber [73], nanogenerators [74] and sensors [75]. To address this demand, scientist have developed various techniques to fabricate nanofiber. Among them electrospinning techniques has been extensively introduced for fiber production.

The main obstacle from moving synthetic nanofibers into end products faces several limitations. One of the main concerns is the very low productivity and very high operating expense. Electrospinning as production platform utilizes high levels of solvents with solution concentrations of up to 94% solvent and 6% polymer which hinder industrial level production, Furthermore, commercially viable electrospinning is limited to high dielectric solvent for its production [76].

Forcespinning® Technique is the new platform for commercial nanofiber production. It uses a very straightforward procedure, centrifugal force to process a polymer solution/melts into micro to nano scale fiber [65]. Moreover, the ability to spin variety of materials from low to high electric constants through revolutionizes the nonwovens techniques of making fiber at high production rate. As the machine revolves the centrifugal force push the viscous solution towards

8

the orifices on each side of the spinneret. When this the polymer jet exits from the orifices, it

forms polymer jet which then stretches to deposit on the prolonged metal collector. Eventually

the ejected jets turn into fiber while solvent evaporates from the polymer jet. The main important

factors that significantly affect for fiber creation are viscosity of solution, humidity and

temperature of the room, evaporation rate, rotating speed, solvents used, distance from collector
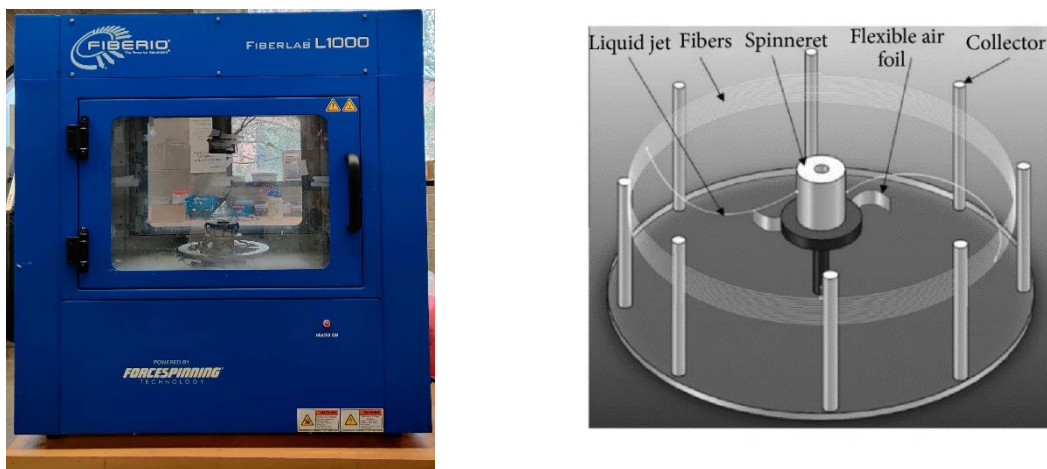
Figure 1: Forcespinning® machines (Cyclone) setup and mechanism of making nanofiber.

Scanning Electron Microscope (SEM)

The scanning electron microscope (SEM) is a microscopy technique which uses a high-

energy electrons focused beam to generate signals at the surface of solid specimens. The sample

information for example morphology, chemical composition, crystal structure and orientation of

solid surface obtained by the interaction between high beam electron and sample surface.

Typically, data are obtained over a specific area of the surface and then morphology is captured

in 2D images. The SEM is capable of determining chemical compositions by EDS as well as

crystalline structure, and crystal orientations through ESBD.

The SEM has following important components: Electron source/Gun, Electron lenses, Sample stage, Electron Detector, Data output representation device. Electrons are produced from electron gun at the top then it is accelerated down through a combination of single/multiple lenses. The sample is mounted in a chamber area which is vacuumed before magnifying the sample. The electron beam position on the sample is controlled by scan coils which are usually mounted
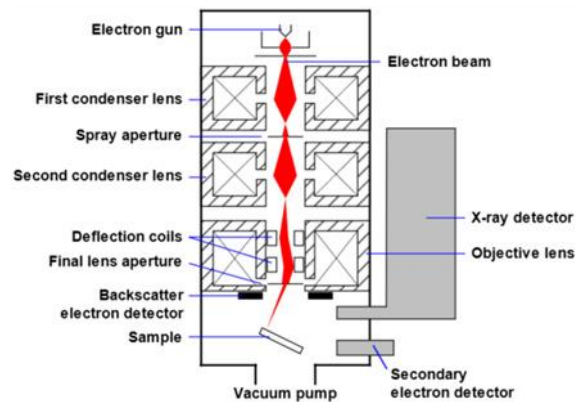
Figure 2: Schematic of a Scanning Electron Microscope.
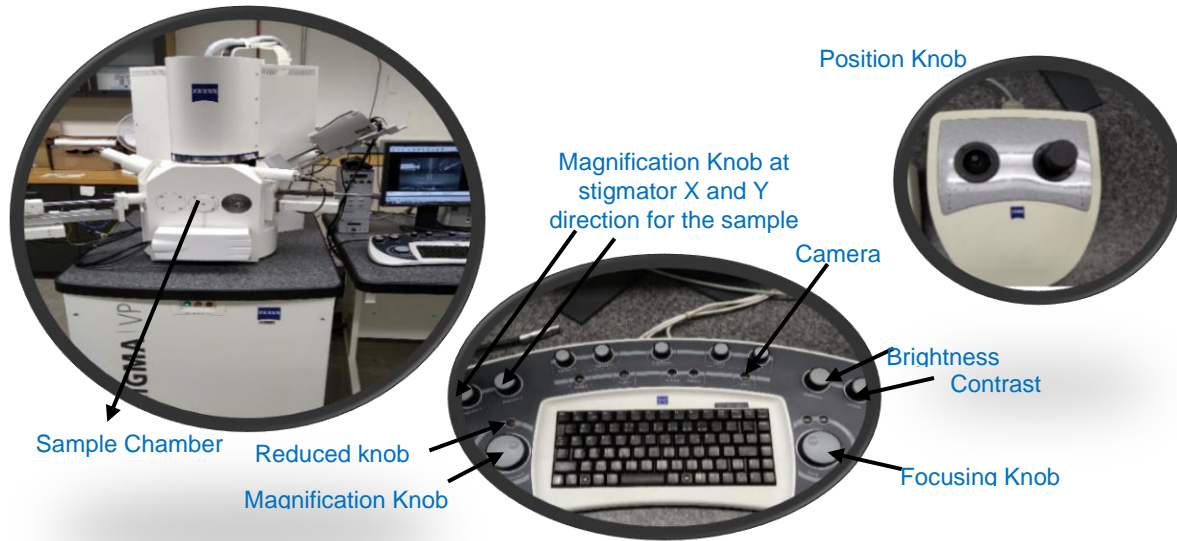
Figure 3: Field emission scanning electron microscope (FESEM) (Sigma VP, Carl Zeiss, Jena, Germany) set up.

Above the objective lens, allow the beam to be scanned over the surface of the prepared samples. Accelerated electron dissipated as variety of signals (secondary electrons, backscattered electrons, X-ray) and among them secondary electrons are used to interact with sample and then detect in the detector to capture the morphology. The samples that are not conductive usually sputtered with metal coat before mounted in sample holder for SEM analysis.

Fourier Transform Infrared Spectroscopy (FTIR)

Fourier transform infrared spectroscopy (FTIR) is a technique which use an infrared spectrum of absorption or emission to analyze a solid, liquid and gas. It applies the Fourier transform to translate the raw data into the actual spectrum. FTIR can be employed to collects

data with high spectral resolution over a wide range, usually between 5000 and 400 cm^{-1} for

mid-IR region, and between 10,000 and 4000 cm^{-1} for near-IR region wavelength.

When infrared radiation is passed through a sample of interest, some portion of the

radiation is absorbed by the sample while some passes through other words transmitted. The

resulting signal received in the detector representing a spectrum which eventually a molecular

'fingerprint' of the sample. The spectra with distinctive pattern illustrate structural characteristics

if the sample molecules.
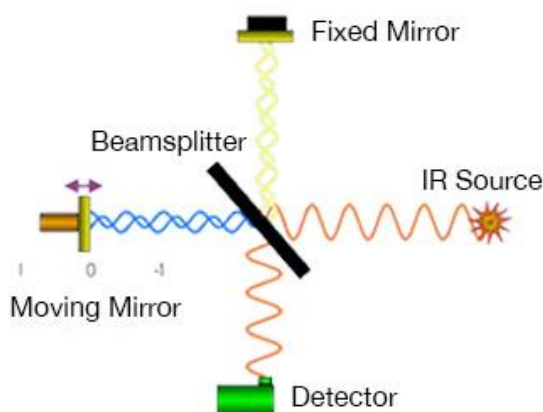
Figure 4: Schematic illustration of FTIR working mechanism.

Oscilloscope

The oscilloscope is a graph-displaying device. Generally, it converts the electrical signal

into graphical output. The oscilloscope has two axes. The vertical (Y) axis represents

voltage/current output signal and the horizontal (X) axis represents time. There are two types od

oscilloscope- analog and digital. Compare to analog oscilloscope, digital oscilloscope uses

analog to digital converter (ADC) to convert the output signal for example voltage/current into

digital information. The signals are generally showed as wave form. Typical oscilloscope has

four different systems – the vertical system, horizontal system, trigger system, and display

system. All these systems combinedly provide the information about a signal and helps to determine predictability and reliability for different applications.
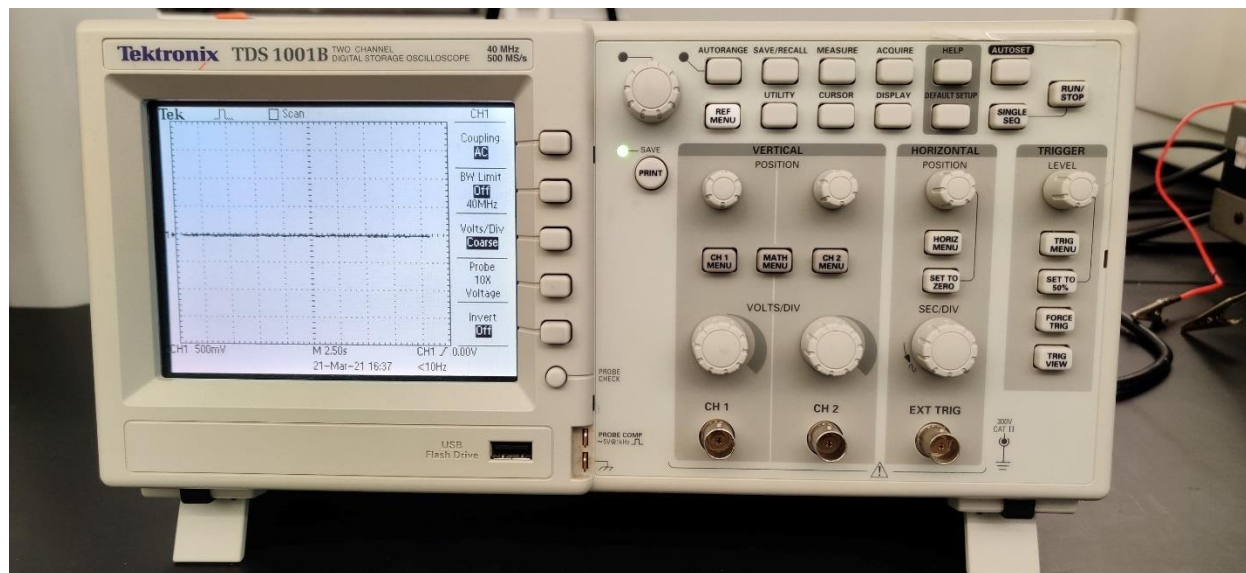
Figure 5: Image of Tektronix TDS 1001B Digital Oscilloscope.

Potentiostat

Potentiostat is actually a voltage sources which vary their output potential in favor to change the resistance across the circuit. Eventually they supply more or less current, yields potential difference across a cell constant thus follow the Ohm's Law. Potentiostat can precisely control the potential of the Counter Electrode (CE) against the Working Electrode (WE) as a result the potential difference between the working electrode (WE) and the Reference Electrode (RE) is fully defined and then the potential difference is showed to the user in a specific value.
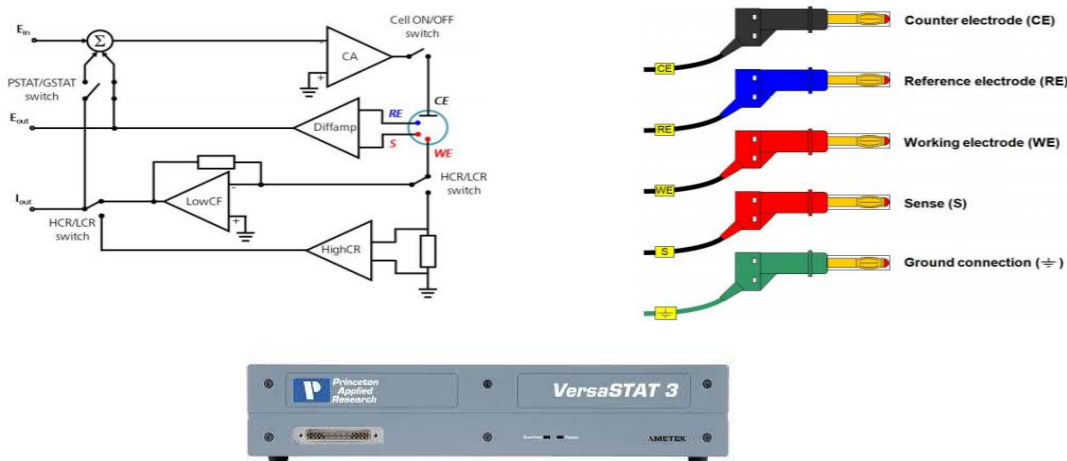
Figure 6: Basic working diagram of a potentiostat, cell cables of a potentiostat and image of VersaSTAT 3 potentiostat.

Here the CE is connected to, Control Amplifier (CA) which is output of an electronic block. Current to flow through the cell due to the force of CA. A Current Follower (LowCF) or Shunt (HighCR) for low and high currents respectively to measure the current flow. The potential difference is measured across the RE and Sense (S).

CHAPTER IV

METHODOLOGY

Fabrication of Nanofiber

The fabrication of a nanofiber involves four important steps: (1) Solution preparation, (2) Injecting the polymer solution in spinneret, (3) Solution spinning, and (3) Collection of prepared nanofibers. All processes are done in controlled environment to avoid environmental contamination.
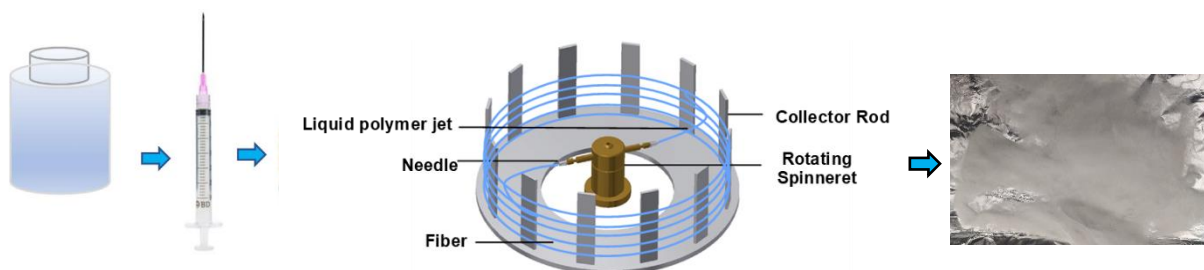
Figure 7: The schematic diagram of fabrication nanofiber by Forcespinning technique and collection of nanofibers.

Materials

Poly [4,4′-methylenebis (phenyl isocyanate)-alt-1, 4-butanediol/di (propylene glycol)/poly caprolactone] which is a methylene-diisocyanate (MDI) thermoplastic polyester/polyether Polyurethane (TPU) was obtained from Sigma-Aldrich. KYNAR 741 polyvinylidene fluoride (PVDF) powder was purchased from Arkema Inc. HPLC grade Acetone (C_3H_6O) and N, N,

Dimethylformamide (DMF, ≥ 99.7%) and Dimethylacetamide (DMA, C_4H_9NO) all were obtained from Fisher Scientific. All the materials were used without any further treatment.

Solution Preparation

In order to make PVDF polymer solution, 1.1 gm PVDF powder was first dissolved in mixture of 2.35 gm DMA and 1.96 gm acetone in 20 ml glass vial. The polymer solution was vortexed for 2 minutes and then mechanically stirred using magnetic stirring at 60°C in silica oil bath for 24 hr. at 800 rpm to ensure complete dissolution. In a similar fashion, to obtain homogenous solution of TPU, the polymer was dissolved in DMF to make 16 wt% mixture. After that the mixture was stirred with magnetic stirrer at 1000 rpm for 48 hours by placing it on silica oil bath at 105°C.

Solution Spinning

The polymer solution mixture was kept at scintillation vials and cooled down until room temperature before using to make the fiber. Later, 2 Ml of independent PVDF and TPU polymer solutions were injected into the Cyclone spinneret equipped with half inch 30-gauge regular needle to spin the fiber. The solution was spined at 5000 rpm for both PVDF and TPU polymer solution. The ejected polymer jet then dried and deposited fiber on the prolonged collectors were then collected in a nonwoven fashion and subsequently stored in HDPE bags to avoid humidity effect containing silica desiccant.

Gold (Au) Coating on TPU Fiber

To fabricate TPU/Au nanofiber membrane, gold (Au) was sputtered using Denton Vacuum Desk II at 50 millitorr pressure for 120 seconds to deposit very thin layer gold coating on one surface of fiber mat.
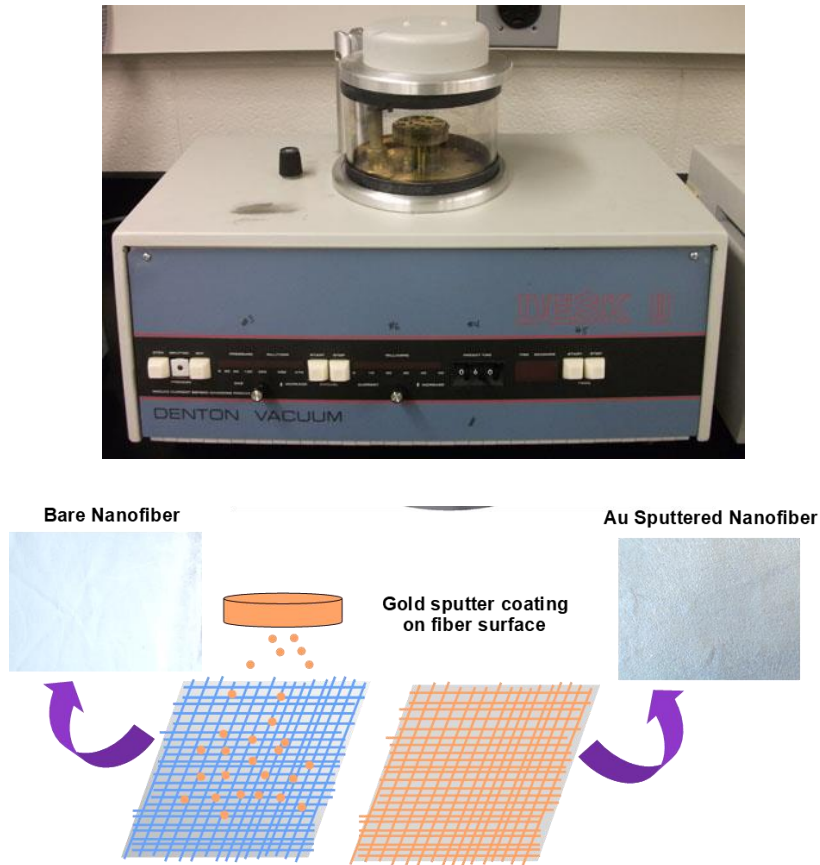
Figure 8: Graphical representation Denton Vacuum DESK II sputter coater and the schematic diagram gold (Au) sputtering on TPU nanofiber.

<center>**Characterization**</center>

The nanofibers were characterized by Scanning electron microscope (SEM), Fourier transfer infrared spectroscopy (FTIR) and Atomic force microscope (AFM) to investigate the fiber morphology and transmittance properties of the fiber.

SEM Characterization

The morphology of the nanofibers was characterized by a field emission scanning electron microscope (FESEM) at an acceleration voltage of 1.0 Kv (Sigma VP, Carl Zeiss, Jena, Germany). To measure fiber diameter Image J software was used. For making fiber diameter distribution 100 counts were taken from the SEM images.

FTIR Characterization

The Fourier Transform Infrared Spectra of the fibers membrane were obtained by using 133 VERTEX 70v FTIR Spectrometer (Bruker) in Attenuated Total Reflection (ATR) mode. The transmittance data of the nanofiber samples were recorded from 450 cm^{-1} to 4000 cm^{-1} wavelengths.

AFM Characterization

AFM measurements were performed on a Bioscope Catalyst AFM (Bruker), mounted on an inverted optical microscope (Ti, Nikon). AFM tapping mode was used for imaging the surface morphology and roughness measurements. Silicon tips with a resonance frequency around 300 kHz, 10 nm in radius, and a spring constant of 40 N/m were selected, and measurements were carried out under ambient conditions and at room temperature.

PVDF-TPU/Au Triboelectric Nanogenerator (TENG)

Fabrication of the TENG

To fabricate the NF-TENG, 1.5×1.25 in^2 fiber mats were cut and attached to commercially available copper (Cu) tape which were acted as electrodes for both positive and negative layer to avoid any airgap between TENG layer and electrode. The two layers of NF-TENG was separated by two polyurethane (PU) spacer of 1.25×0.25 in^2 on both ends of the NF-TENG that were attached to the fiber membrane with carbon black tape prevents each layer from continually touching each other. An extension of Cu tape was added with each electrode for attaching the device with alligator clips. A layer of PLA was attached on the outer side of both electrodes to impart structural support. All the experimental works were done in ambient condition.

■ PLA   ■ Electrode (Cu)   ■ TPU/Au Nanofiber   ■ PVDF Nanofiber   ■ Spacer (PU)
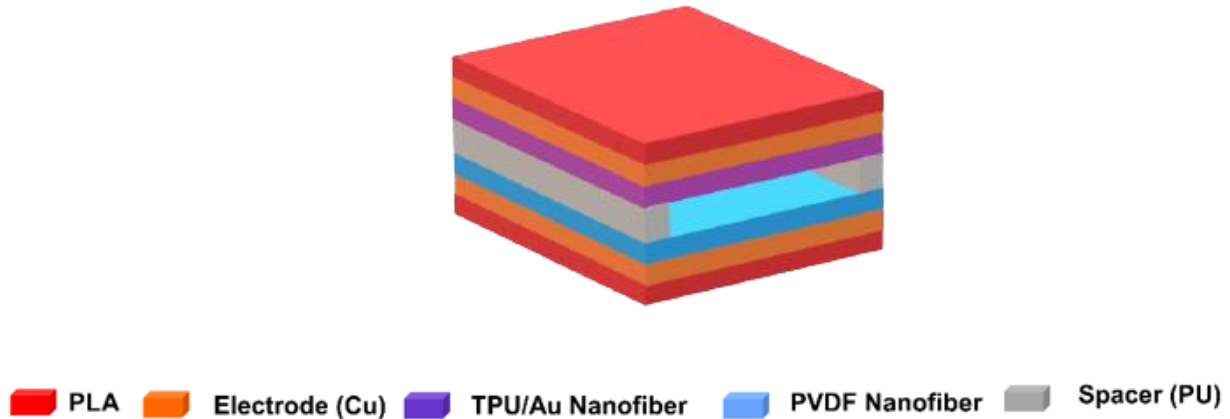
Figure 9: Schematic of PVDF-TPU/Au Nanofiber based Triboelectric Nanogenerator.

Mechanism of TENG

The working principle of NF-TENG showed in Figure 2. Usually a TENG require two electrification layers and initially these two layers were in (a) contact mode with no with elector flow [12]. However, later the two layers were periodically pressed and as the PVDF membrane is triboelectrically negative than TPU, when the layers got released (b), the charge was ejected from

TPU/Au layer [35]. Due to the high electron affinity of PVDF, the ejected electron flow to the PVDF fiber leaving net negative charges in PVDF layer [77], [78]. This separation induced a potential difference across the two layers resulted current to flow through the external circuit connected to the Cu tape electrodes. When the fiber layers got fully separated (c) the open circuit voltage were decreased and became zero [79]. The electricity flow became reversed (d) as the layers again brought closer to each other [80].
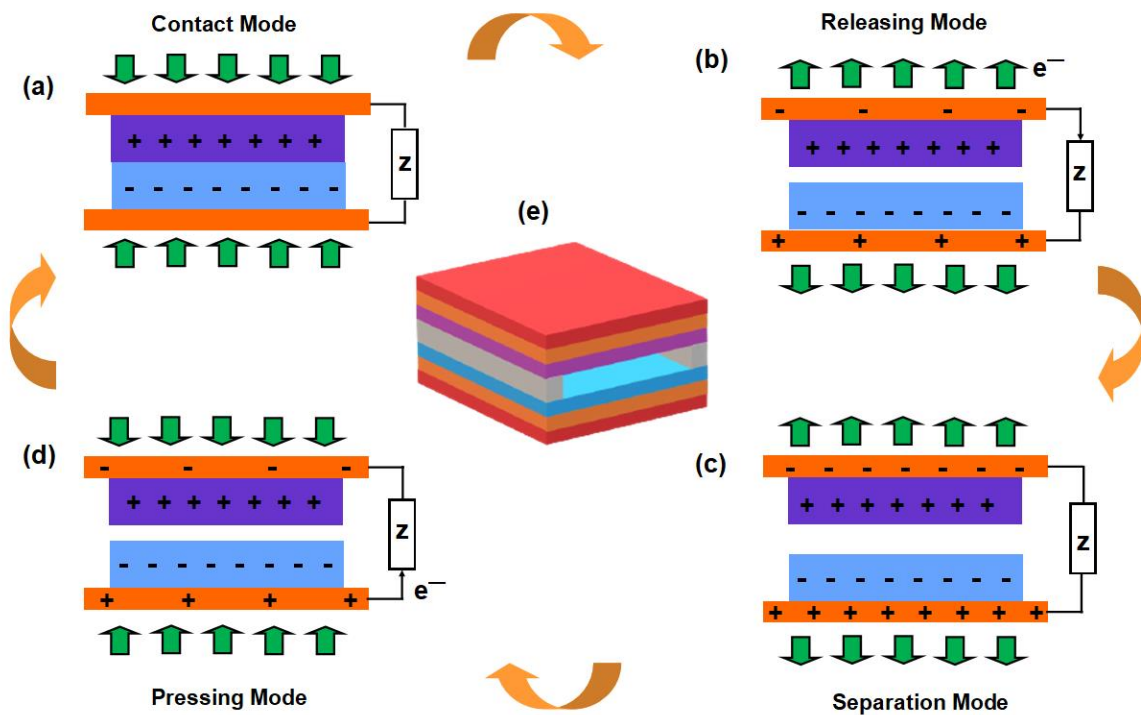
Figure 10: Schematic of NF-TENG energy generation process.

Measuring Electrical Performance of TENG

The open circuit outputs voltage of the NF-TENG were measured by Tektronix TDS1001B digital oscilloscope. However, for recoding current output, the signal was measured using the oscilloscope along with low noise current preamplifier (Stanford Research SR570). For capacitor

and body motion sensing tests, the output voltage was measured using VersaSTAT 3 potentiostat

while electrical connectors were attached to the nanogenerator electrodes.

CHAPTER V

RESULTS AND DISCUSSION

SEM Morphological Analysis of Nanofiber Membrane

The morphology of the force spun PVDF and TPU nanofiber can be highlighted by scanning electron microscopy in figure 11 (a) and (b).
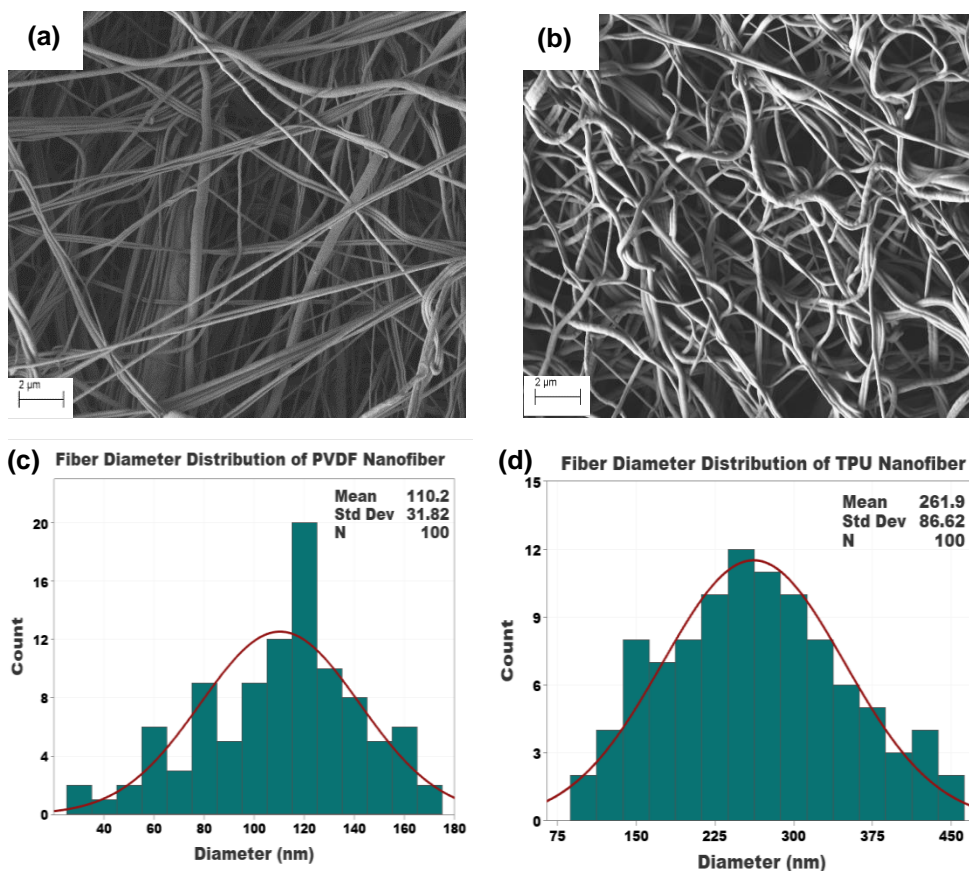
Figure 11: FESEM images (a and b) and fiber diameter distribution (c and d) of PVDF and TPU nanofibers.

The images illustrate that PVDF fibers align more closely compare to PVDF fiber which resulted less permeability and more surface area compare to TPU nanofiber. The surface morphology of PVDF NFs were found smoother while the TPU fibers were more twisted in nature. From figure 11 (c) and (d) the fiber diameter histogram, it can be accounted that the average fiber diameter of PVDF nanofiber was 110 nm while TPU nanofibers were comparatively thicker with average fiber diameter of 262 nm

FTIR Analysis of Nanofiber Membrane

The fibers were further investigated by Fourier Transform Infrared Spectroscopy (FTIR) in figure 12. The characteristic bands of β phase PVDF in figure 12 (a) identified as 877 cm^{-1}, 1172 cm^{-1} and 1401 cm^{-1}. The stretching around 877 cm^{-1} and 1072 cm^{-1} peaks were due to C-C bond skeletal vibration of β PVDF [81], [82]. Peaks at 510 cm^{-1} attributed to the –CF2 bending [83]. The peaks observed at 1172 cm^{-1} and 1401 cm^{-1} were due to the stretching vibration C-F and C-H group respectively while The band at 839 cm^{-1} assigned to a mixed mode of –CH2 rocking and –CF2 asymmetric stretching vibration [81], [83]. These β phases of the PVDF nanofiber escalated more triboelectricity in the nanogenerator. The spectrum in figure 12 (b) revealed that TPU membrane absorption band at 3325 cm^{-1} was due to the N-H stretching vibration in the urethane group whereas 1415 cm^{-1}, 2862 cm^{-1} and 2938 cm^{-1} were corresponded to – CH2– asymmetric stretching vibration [84]–[86]. The other characteristics sharp peak at 1726 and 1701 cm-1 were associated with stretching vibration of the carbonyl group (C=O) in the amide while stretching at 1597 cm^{-1} caused by N-H group flexural absorption [86]. The band around 1067 cm^{-1} and 1217 cm^{-1} were identified by C–O bond stretching[85].
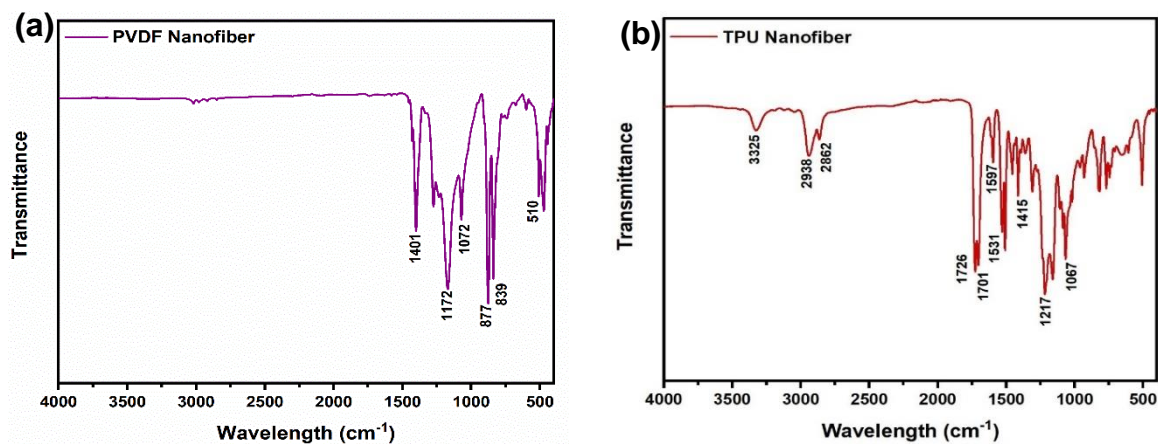
Figure 12: FTIR spectrum of (a) PVDF and (b) TPU nanofiber.

AFM Morphological Analysis of Nanofiber Membrane

Fibers were imaged using AFM tapping mode, which produces three type of images, height, deflection, and phase. Here we are presenting the deflection and phase images because they provide more information about the surface morphology compared to the height image. Figure 13(a) is an AFM deflection image of the PVDF fiber, showing a smooth morphology made of several nanofibers clearly visible on the phase image (arrow, Figure 13(b)). The inset in figure 13(a) is a 3D image of the fiber where the nanofibers are visible. The average value of the roughness of the top surface of the fiber is 17.42 ± 2.34 nm (n =10 measurements)

Figure 13(c) is an AFM deflection image of the TPU fiber, showing smooth morphology as well without any visible nanofiber as in the PVDF fiber. This is confirmed in the phase image (figure 13(d)), where the top surface of the fiber looks very homogenous. In addition, the 3D image (inset figure 13(c)) does not show any specific features on the top surface of the fiber. However, the average roughness of the fiber almost doubled compare to the PVDF one, 31.1 ± 2.73 nm (n = 10 measurements).
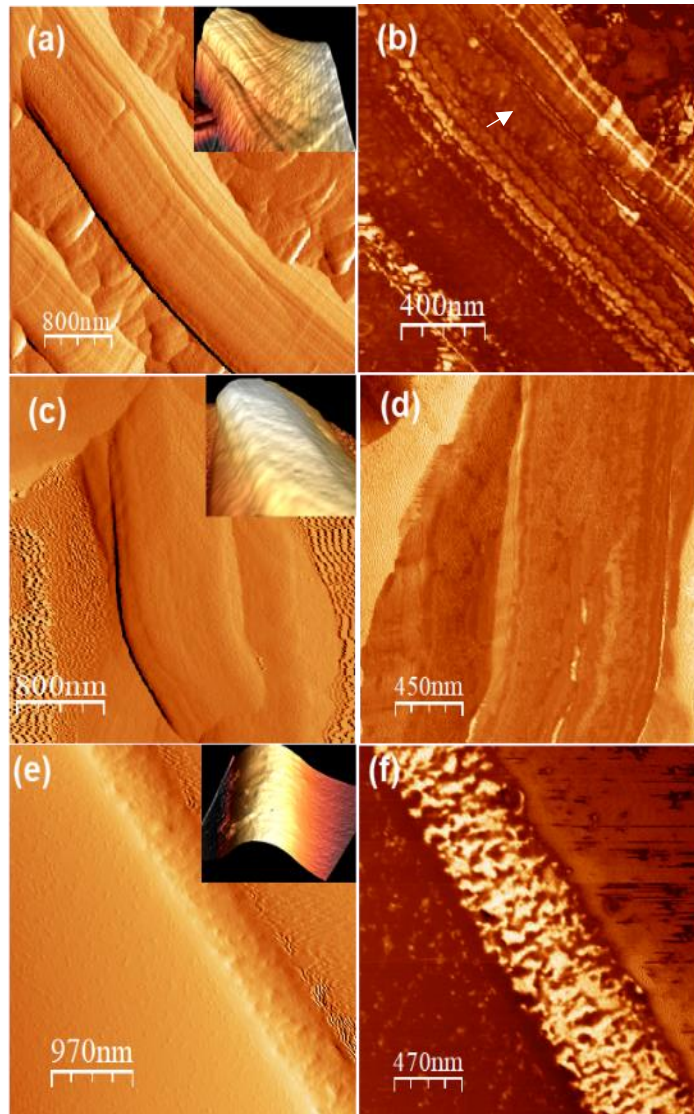
Figure 13: AFM morphology of (a-b) PVDF nanofiber, (c-d) TPU nanofiber and (e-f) gold sputtered TPU (TPU/Au) nanofiber.

Figure 13(e), is an AFM deflection image of the TPU/Au fiber, showing a homogenous but quite different surface structure compared to the two other fibers. The presence of the nanoparticles on the surface of the fiber is clearly visible and are homogenously distributed. This data is confirmed with the phase image (figure 13(f)), where a white structure is the most dominant. In AFM, phase images the white areas represent harder structure that can be associated with the gold

nanoparticles in our case. This is also visible in the 3D image of the fiber (inset figure 13(e)).

Accordingly, the average surface roughness of the fiber was also increased to 47.73 ± 3.25 nm.

Measuring Open Circuit Voltage (V_{OC}) and Short Circuit Current (I_{SC})

To inspect the electrical performance of PVDF-TPU/Au NF-TENG (PTA-TENG), we used continuous finger tapping at 60 bpm (1 Hz), 120 bpm (2 Hz), 180 bpm (3 Hz), and 240 bpm (4 Hz) load frequency [87], [88]. The vertical tapping movement of the TENG generated triboelectricity effect resulted alternating current (AC) open circuit voltage (V_{OC}) and short circuit current (I_{SC}) were highlighted in figure 14. The results indicate that both V_{OC} and I_{SC} increased with the increasing load frequency[89]. The maximum V_{OC} recorded for PTA-TENG were 130, 165, 230 and 254 V for 60, 120, 180 and 240 bpm load frequency respectively while the highest I_{SC} obtained were 42, 52.5 ,72 and 86 μA for 60, 120, 180 and 240 bpm.
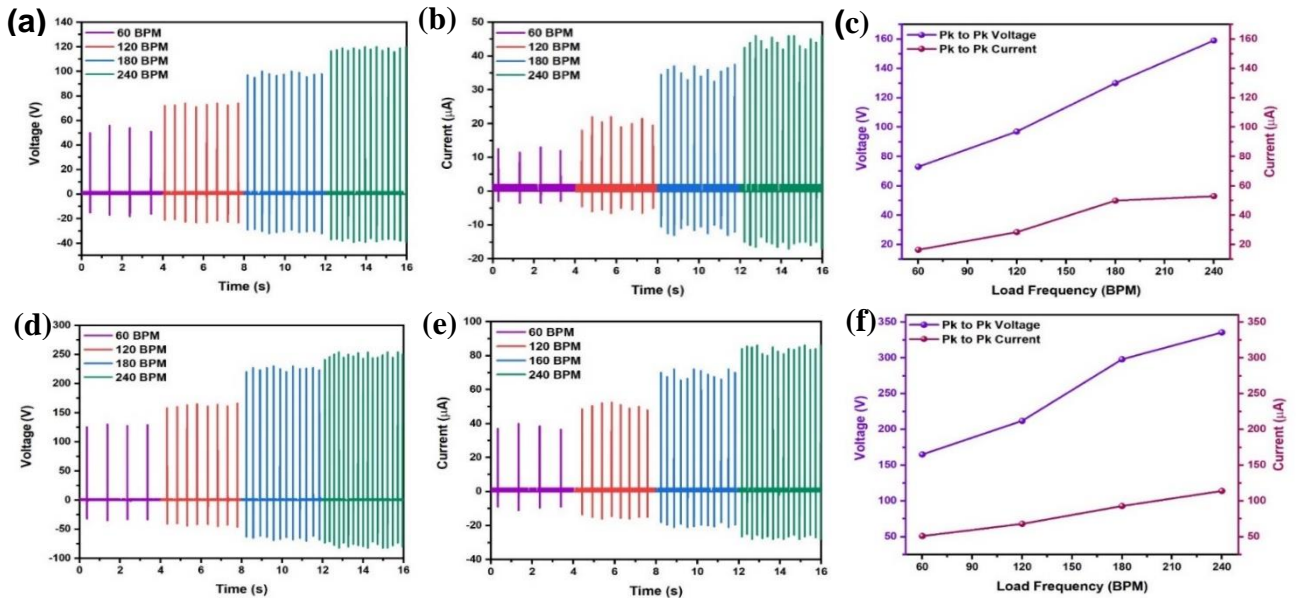
Figure 14: Electrical performance of NF-TENG. (a) & (d) Open circuit voltage; (b) & (c) Short circuit current; (c) & (f) Maximum peak to peak voltage and current output for PVDF-TPU NF-TENG and PVDF-TPU/Au NF-TENG respectively for 60, 120, 180, 240 bpm load frequency.

26

Furthermore, the outputs were then compared with bare PVDF-TPU nanofiber based TENG. The highest AC open circuit short voltage and short circuit current reported was 120 V and 46 µA at 240 bpm load frequency which signified that the effect of Au on the surface or TPU nanofiber improved the output performance by 112% and 86% respectively for open circuit voltage and short circuit current (Fig. 14 (d) & (e). From the figure 14 (c) and (f), it can be interpreted that maximum peak to peak voltage and current achieved for gold sputtered TPU based TENG was 336 V and 114 Ma that significantly higher than normal TPU-PVDF nanofiber based TENG, yielded only 159 V and 53 Ma at 240 bpm load frequency.

Measuring Constant Pressure V_{OC} and I_{SC}

Moreover, to further investigate the PTA-TENG performance with constant pressure using vertical punch machine (Fig. 15 (c)), we varied the load from 10 Psi to 30 Psi (pound per square inch) at 65 bpm frequency, the output signal showed similar results like finger tapping but this time more uniform peak was evident [90], [91]. As the applied pressure got higher, the force impact due to the punch increased on the triboelectric surface and the output AC V_{OC} observed were 24, 40, 66, 92 and 128 volts for 10, 15, 20, 25 and 35 Psi (Fig. 15 (a)). Besides, the output current signals were also increased linearly and yielded 6.7, 11.4, 20.35, 27.75 and 35.6 µA short circuit current for 10, 15, 20, 25 and 30 Psi respectively (Fig. 15 (b)). However, the output V_{OC} and I_{SC} achieved during pressure test were quite smaller compare to finger tapping test as the punch effective contact area was only 0.7854 in^2 with circular punch diameter 1 inch (Fig. 15 (d)), while during finger tapping, the active triboelectric surface area was 1.25 in^2 (1.25 × 1.0 in^2).
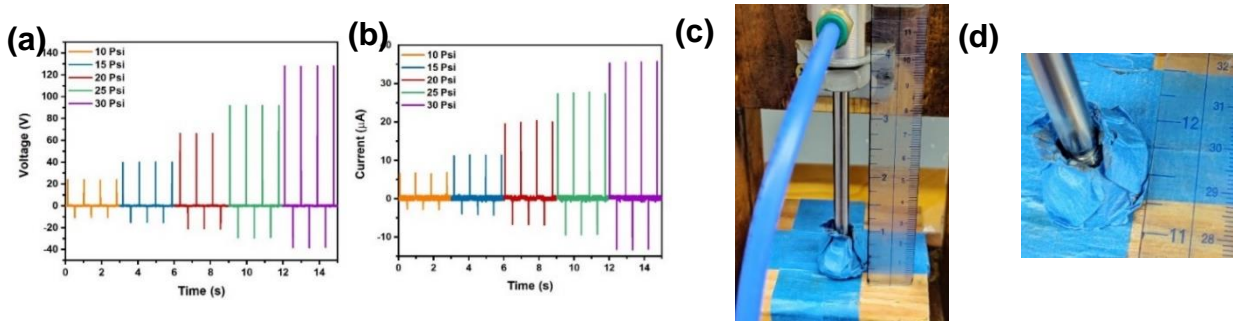
Figure 15: Electrical performance of PVDF-TPU/Au NF-TENG. (a) Open circuit voltage, (b) Short circuit current output, (c) Experimental set up for fixed pressure test for different pressure at 65 bpm load frequency and (d). Punch dimension.

Measuring Performance of Full Bridge Rectification

The output performance of the PTA-TENG was also examined attaching a full wave bridge rectifier with it (Fig. 16 (a)) [33], [77]. The figure 15 (b) shows the ability to rectify the output AC signal of the PTA-TENG to full wave DC voltage by finger tapping at 240 bpm load frequency. The output voltage signals were uniform in nature with only positive voltage DC was evident and the maximum voltage recorded was 152 V.
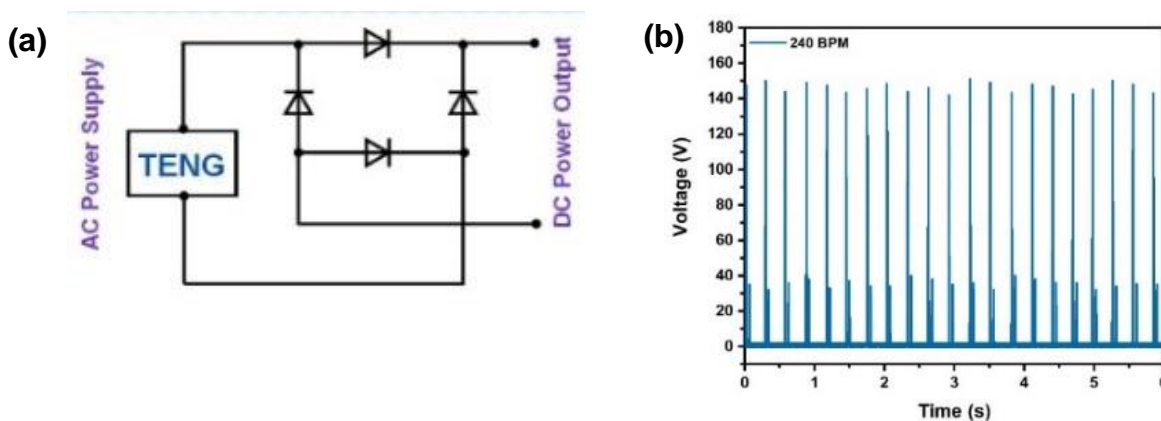
Figure 16: Electrical performance of NF-TENG. (a) Full bridge rectifier circuit. (b) Rectified DC voltage output

Measuring Capacitor Charging Test

In contrast to electrical performance, the chagrining ability of the PTA-TENG was also investigated with different capacitor to demonstrate future prospect of storing and charging small electronic devices [12], [64]. Capacitor typically used for small electronic device and the Figure 17 (a) demonstrates the schematic view of the capacitor circuit with a full bridge rectifier attaching to the TENG cell used in the experiment. The capacitor with 1.0, 3.3, 4.7, 6.8 and 10.0 µF capacitance were employed to charge the open circuit voltage for 30s at 240 bpm load frequency with finger tapping (Fig. 17 (b)). The curves show that as the capacitance got higher, the rate of charging capacity gradually decreased. The maximum output charged voltage observed for above mentioned capacitors were 7.64, 6.03, 4.97, 3.26 and 1.95 V respectively.
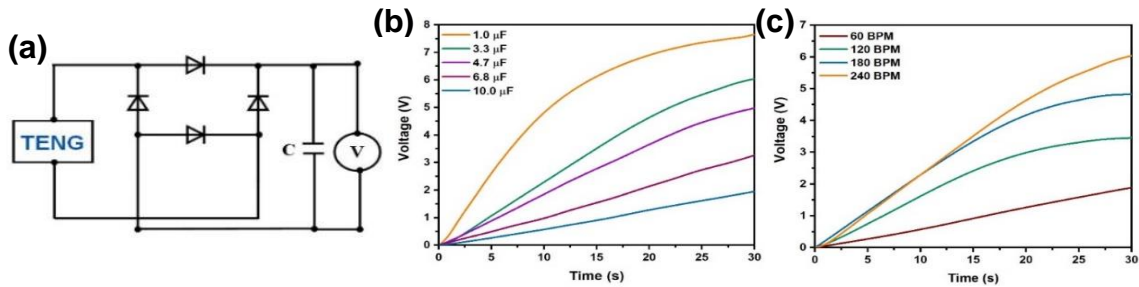
Figure 17: Electrical performance of NF-TENG. (a) Capacitor test circuit, (b) Charging ability of NF-TENG with different capacitors, (c) Charging with 3.3 Mf capacitor for different bpm load frequency.

Furthermore, after examining with different capacitors, the PTA-TENG was further experimented with 3.3 µF capacitor but this time with varying load frequency. From the figure 16 (c), it can be highlighted that for constant 30s tapping mode, output charged voltage got higher as load frequency varied from 60 to 240 bpm. The highest voltage recorded 6.03 V at 240

bpm where 60 bpm load frequency derived only 1.89 V which illustrated that higher charging

voltage can be achieved with at high load frequency [87].

Measuring External Resistance Load Test

Figure 18 (a) represents the external resistance load connected in series with the full

bridge rectified nanogenerator. From the figure 18 (b), it can be elucidated that the instantaneous

average voltage output showed gradual increase while the average current output indicated

opposite trend with varying resistive load from 5 KΩ to 10 MΩ at a frequency of 4 Hz (240

bpm) following the Ohm's law [77], [92]. According to the maximum power transfer theorem,

the maximum power output achieved when the internal impedance of the TENG sync with the

external load [33]. Very sharp voltage output rise was observed from 1MΩ to 6.5 MΩ. As a

result, the power ($P = U^2/R$) increased initially (figure 18 (c)) and reached maximum 2.13 Mw at

6.5 MΩ load resistance and then gradually started to decrease.
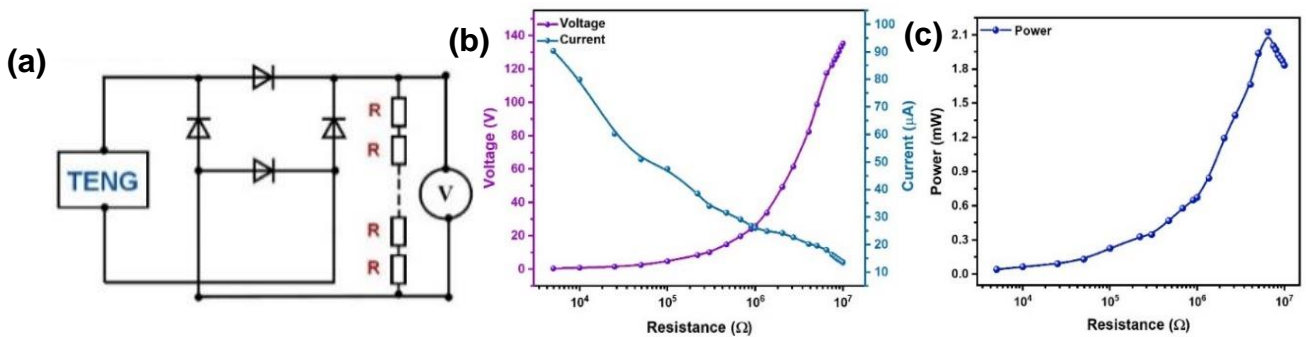
Figure 18: Electrical performance of NF-TENG. (a) Resistance test circuit, (b) Average voltage

and current and (c) power output of PVDF-TPU/Au NF-TENG with different external resistance.

Light Emitting Diode Test

Moreover, to demonstrate the practicability of our nanogenerator, we illuminated 75 LED

with high brightness shown in the [93]. The TENG was attached with series of commercial LEDs

(1.5 V each) through a full bridge rectifier with a 0.1 µA capacitor and the nanogenerator was

hand tapped to light the up the LEDs (figure 19 (a)). This high power output and LED test of the

TPA-TENG demonstrated a very promising potential to power flexible and wearable electronics

[94], [95].
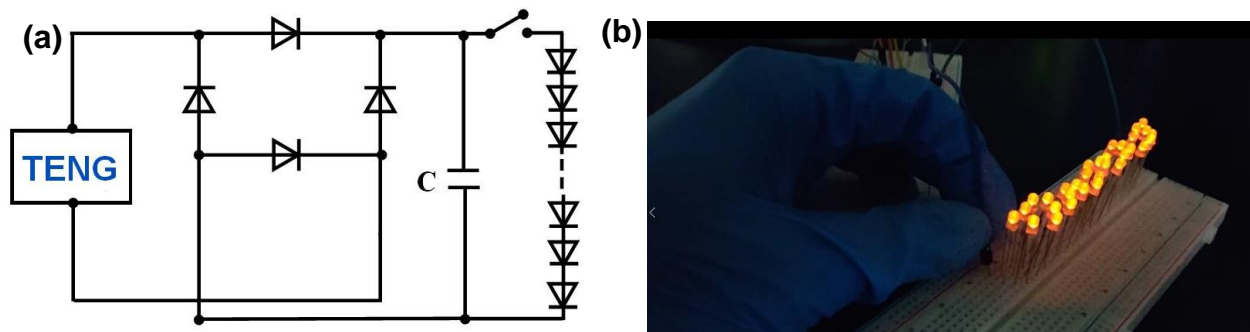
Figure. 19: Electrical performance of NF-TENG. (a) Schematic circuit diagram of LED test (b)

Photographic representation of lighting up LEDs with PTA-TENG

Bicep Muscle Contraction Sensing Test

After investigating the energy storage capability of PTA-TENG, the nanogenerator was
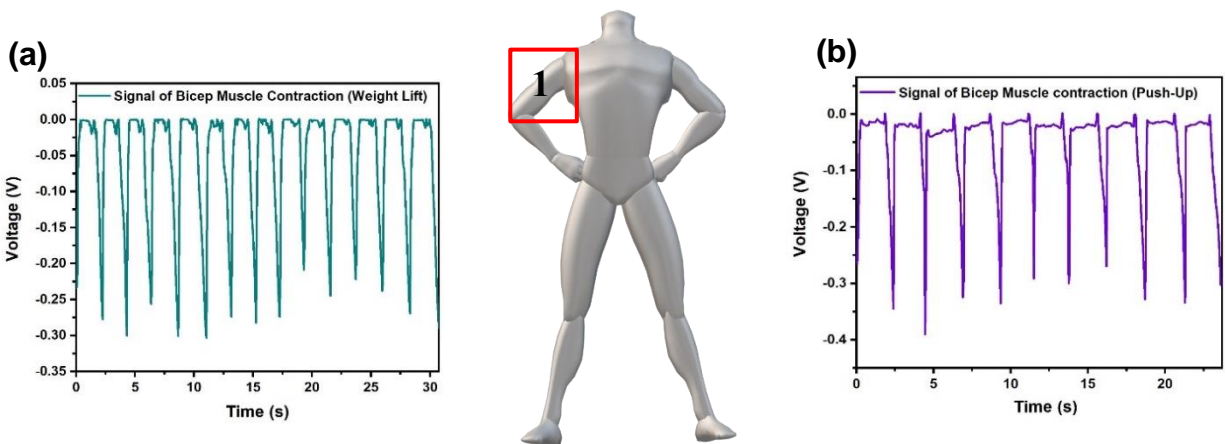
Figure. 20: Signal of bicep muscle contraction for (a) 5 lb weight lift (b) incline push up.

explored for various biomechanical motion sensing applications as shown in figure 20. During the 5lb weight lift (figure 20 (a)) and incline push up (figure 20 (b)), the bicep muscle contraction was recorded as AC open circuit voltage signal (~0.25 – 0.35 V peak) which signified superior bending sense capability of the proposed sensor.

Respiration Sensing Test

The sensor was further examined to detect respiration rate at normal breathing and rapid breathing during running (figure 21). The results show sinusoidal signal for the inhale and exhale motion by attaching the TENG at the chest. As the sensor was prepared by nanofiber air could easily penetrate the fiber membrane.
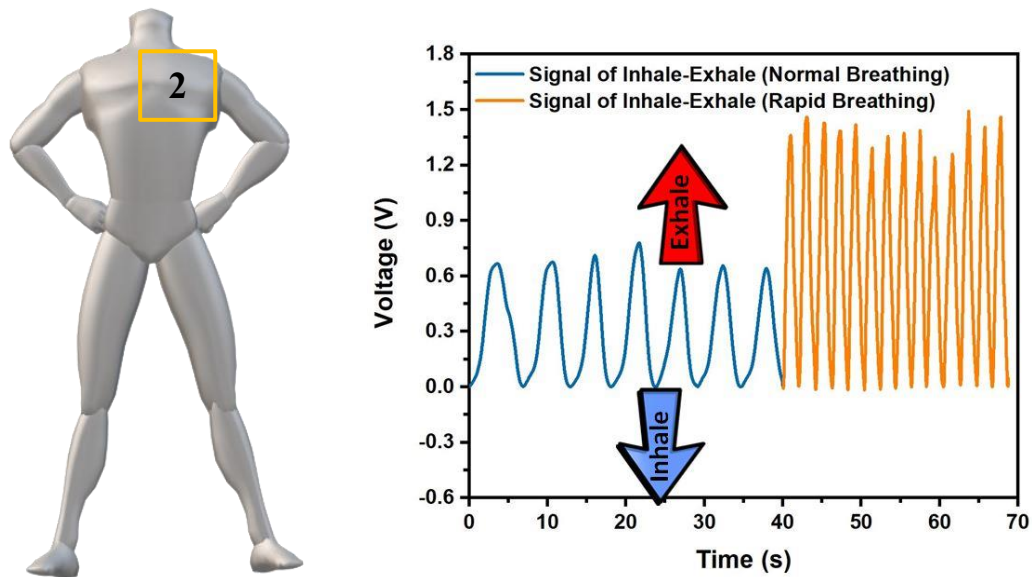
Figure. 21: Signal of normal breathing and rapid breathing.

Forearm Muscle Contraction Sensing Test

Similar to bicep contraction, the PTA-TENG sensor was also investigated for different hand gesture: one by one finger opening and then closing altogether (figure 22 (a)) and fist opening

32

and closing (figure 22 (c)) at 1 Hz frequency. The distinct peak in figure (figure 22 (b)) clearly showed for how many fingers were opened or closed at a given time. The output voltage signals were generated by the pressure drop across two friction TENG layers. The fist opening and closing responses were repetitive (~1.8 V peak) and distinctive and moreover, output looked like twisted pulsed signal. The forearm muscle contraction test was also done for wrist rotation (clockwise direction) in figure 22 (d) at 60 bpm load frequency and similar pattern of signal was depicted at regular time interval.
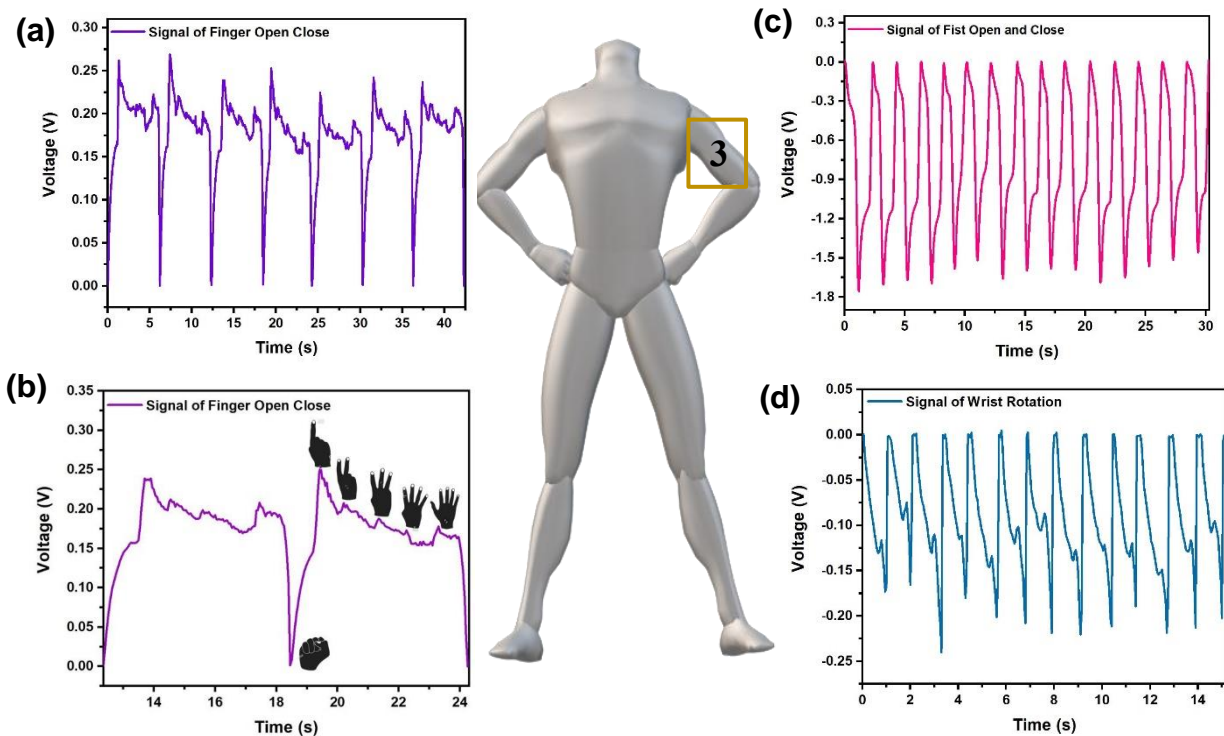
Figure. 22: Signal from forearm muscle contraction for (a) finger gradual open close (b) magnified signal of finger open close, (c) fist open close and (d) wrist rotation.

Quadricep Muscle Contraction Sensing Test

The TENG sensor was then attached to the front part of the leg, just above the knee, near the quadricep muscles, to capture the motion of the muscle contraction and expansion. The results

from the bending of leg to 90 degrees from standing position in figure 23 (a) was quite similar to bicep contraction, but the peaks were intense (~2.4 V). The quadricep contraction was also captured during slow jogging and running illustrated in figure 23 (b). In both cases the signals were same but only varied in respect to V_{OC} peak intensity as in case of running the V_{OC} peaks were ~2.0 V, double than slow jogging. The reaction from different body motion gestures clearly indicated real life self- power sensor capability. Consequently, our proposed PTA-TENG was able to evaluate physiological information meticulously while charging small electronics simultaneously.
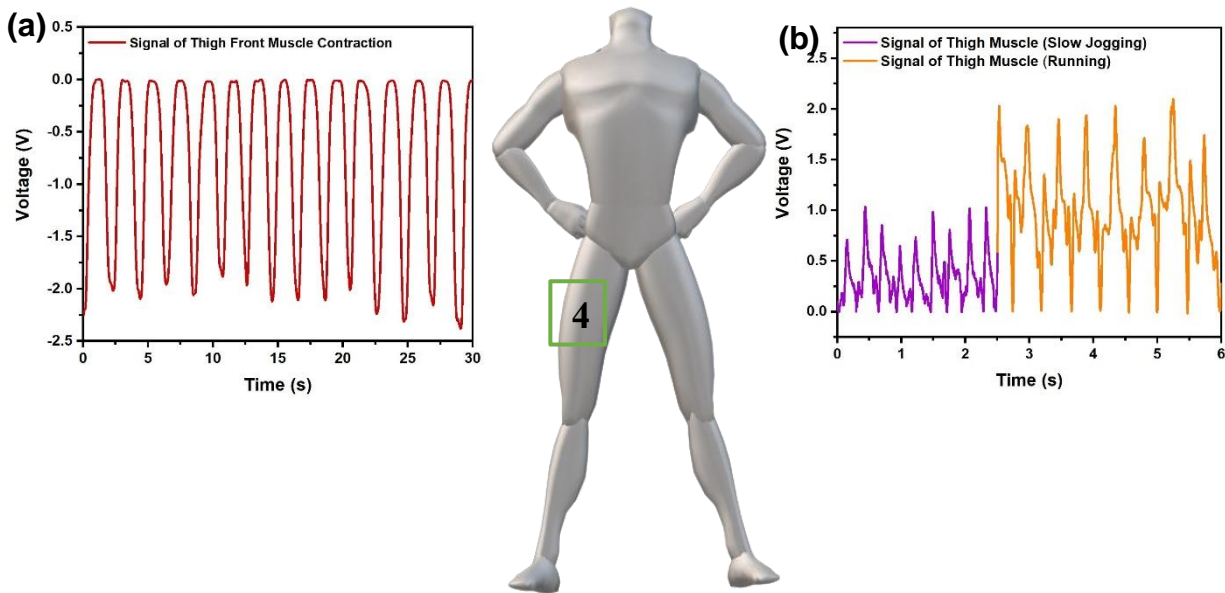
Figure. 23: Thigh muscle (quadricep) contraction signal for (a) leg up-down movement and (b) slow jogging and running.

CHAPTER VI

CONCLUSION

In summary, Forcespinning technique has been introduced for the first time to synthesize triboelectric fiber membrane layers. The improved electrification properties of force spun fibers due to the β phase domination in PVDF nanofiber which resulted from the unidirectional mechanical stretching during fiber formation. Apart from this, we sputtered gold coating on the TPU nanofiber surface to further improve the electrical performance. This simple surface modification with extra frictional surface yielded in noticeable electrical output of 254 V open circuit voltage and 86 µA short circuit current which were 2.12 and 1.87 times greater than bare TPU/PVDF nanofiber based TENG. Constant pressure tests were also done to illustrate the capability of uniform signal output in comparison to finger tapping mode. The capacitor charging test of the modified TENG offered a quick charging capability of maximum 7.64 volt within 30 seconds of period using 1.0 µF capacitor which indicates the great promise of the proposed TENG for charging small electronics. Besides, varying external resistance load from 5 KΩ to 10 MΩ, we obtained significant 2.13 mW power from a small TENG with an active contact area of only 1.25 in^2 which eventually implied prospects of our prepared TENG for small but high-density power source. The real-life applicability of the TENG was explored by illuminating 75 commercial LED by only 12 seconds of hand tapping. The nanogenerator was further analyzed for sensory application by connecting to different body parts namely forearm, quadricep muscle, chest and it demonstrated an attractive capability for distinct human biomechanical motion sensing application.

REFERENCES

[1] K. Parida *et al.*, "Extremely stretchable and self-healing conductor based on thermoplastic elastomer for all-three-dimensional printed triboelectric nanogenerator," *Nat. Commun.*, vol. 10, no. 1, 2019, doi: 10.1038/s41467-019-10061-y.

[2] L. Bai *et al.*, "Review Article Biopolymer Nanofibers for Nanogenerator Development," vol. 2021, 2021.

[3] L. Xie, N. Zhai, Y. Liu, Z. Wen, and X. Sun, "Review Article Hybrid Triboelectric Nanogenerators : From Energy Complementation to Integration," vol. 2021, 2021.

[4] C. Wang *et al.*, "Wearable Wire-Shaped Symmetric Supercapacitors Based on Activated Carbon-Coated Graphite Fibers," *ACS Applied Materials and Interfaces*, vol. 10, no. 40. pp. 34302–34310, 2018, doi: 10.1021/acsami.8b12279.

[5] Y. Zheng *et al.*, "An electrospun nanowire-based triboelectric nanogenerator and its application in a fully self-powered UV detector," *Nanoscale*, vol. 6, no. 14, pp. 7842–7846, 2014, doi: 10.1039/c4nr01934b.

[6] T. Huang, M. Lu, H. Yu, Q. Zhang, H. Wang, and M. Zhu, "Enhanced power output of a triboelectric nanogenerator composed of electrospun nanofiber mats doped with graphene oxide," *Sci. Rep.*, vol. 5, no. September, pp. 1–8, 2015, doi: 10.1038/srep13942.

[7] Y. Hao, Y. Bin, H. Tao, W. Cheng, W. Hongzhi, and Z. Meifang, "Fluoride (PVDF) Triboelectric Nanogenerator via Electrospinning," in *2015 IEEE 15th International Conference on Nanotechnology (IEEE-NANO)*, 2015, vol. 1, pp. 1485–1488, [Online]. Available: doi: 10.1109/NANO.2015.7388923.

[8] S. Park, M. Seol, S. Jeon, D. Kim, D. Lee, and K. Choi, "Surface Engineering of Triboelectric Nanogenerator with an Electrodeposited Gold Nanoflower Structure," *Nat. Publ. Gr.*, no. July, pp. 1–7, 2015, doi: 10.1038/srep13866.

[9] D. W. Kim, J. H. Lee, J. K. Kim, and U. Jeong, "Material aspects of triboelectric energy generation and sensors," *NPG Asia Mater.*, 2020, doi: 10.1038/s41427-019-0176-0.

[10] B. Dudem, D. H. Kim, and J. S. Yu, "Triboelectric nanogenerators with gold-thin-film-coated conductive textile as floating electrode for scavenging wind energy," 2017, doi: 10.1007/s12274-017-1609-0.

[11] M. Mariello *et al.*, "Novel Flexible Triboelectric Nanogenerator based on Metallized Porous PDMS and Parylene C," pp. 1–12, 2020.

[12] H. J. Qiu *et al.*, "A calibration-free self-powered sensor for vital sign monitoring and finger tap communication based on wearable triboelectric nanogenerator," *Nano Energy*, vol. 58,

no. January, pp. 536–542, 2019, doi: 10.1016/j.nanoen.2019.01.069.

[13] S. Zhao *et al.*, "All-Nanofiber-Based Ultralight Stretchable Triboelectric Nanogenerator for Self-Powered Wearable Electronics," *ACS Appl. Energy Mater.*, vol. 1, no. 5, pp. 2326–2332, 2018, doi: 10.1021/acsaem.8b00439.

[14] F. Chen *et al.*, "A novel triboelectric nanogenerator based on electrospun polyvinylidene fluoride nanofibers for effective acoustic energy harvesting and self-powered multifunctional sensing," *Nano Energy*, vol. 56, pp. 241–251, 2019, doi: 10.1016/j.nanoen.2018.11.041.

[15] J. Shen, Z. Li, J. Yu, and B. Ding, "Humidity-resisting triboelectric nanogenerator for high performance biomechanical energy harvesting," *Nano Energy*, vol. 40, no. July, pp. 282–288, 2017, doi: 10.1016/j.nanoen.2017.08.035.

[16] W. Liu, M. S. Song, B. Kong, and Y. Cui, "Flexible and Stretchable Energy Storage: Recent Advances and Future Perspectives," *Adv. Mater.*, vol. 29, no. 1, 2017, doi: 10.1002/adma.201603436.

[17] M. Armand, "Nature Lithium Battery," *Nature*, vol. 414, no. November, pp. 359–367, 2001, [Online]. Available: http://www.ncbi.nlm.nih.gov/pubmed/11713543.

[18] Y. Wang, Y. Yang, and Z. L. Wang, "Triboelectric nanogenerators as flexible power sources," *npj Flex. Electron.*, vol. 1, no. 1, pp. 1–9, 2017, doi: 10.1038/s41528-017-0007-8.

[19] T. Huang, C. Wang, H. Yu, H. Wang, Q. Zhang, and M. Zhu, "Human walking-driven wearable all-fiber triboelectric nanogenerator containing electrospun polyvinylidene fluoride piezoelectric nanofibers," *Nano Energy*, vol. 14, pp. 226–235, 2014, doi: 10.1016/j.nanoen.2015.01.038.

[20] Y. Yang *et al.*, "Pyroelectric nanogenerators for harvesting thermoelectric energy," *Nano Lett.*, vol. 12, no. 6, pp. 2833–2838, 2012, doi: 10.1021/nl3003039.

[21] Y. Zi *et al.*, "Triboelectric-pyroelectric-piezoelectric hybrid cell for high-efficiency energy-harvesting and self-powered sensing," *Adv. Mater.*, vol. 27, no. 14, pp. 2340–2347, 2015, doi: 10.1002/adma.201500121.

[22] H. Y. Mi, X. Jing, M. A. B. Meador, H. Guo, L. S. Turng, and S. Gong, "Triboelectric Nanogenerators Made of Porous Polyamide Nanofiber Mats and Polyimide Aerogel Film: Output Optimization and Performance in Circuits," *ACS Appl. Mater. Interfaces*, vol. 10, no. 36, pp. 30596–30606, 2018, doi: 10.1021/acsami.8b08098.

[23] Z. Saadatnia, S. G. Mosanenzadeh, E. Esmailzadeh, and H. E. Naguib, "A High Performance Triboelectric Nanogenerator Using Porous Polyimide Aerogel Film," *Sci. Rep.*, vol. 9, no. 1, pp. 1–12, 2019, doi: 10.1038/s41598-018-38121-1.

[24] F. R. Fan, Z. Q. Tian, and Z. Lin Wang, "Flexible triboelectric generator," *Nano Energy*, vol. 1, no. 2, pp. 328–334, Mar. 2012, doi: 10.1016/j.nanoen.2012.01.004.

[25] Y. Kim, X. Wu, and J. H. Oh, "Fabrication of triboelectric nanogenerators based on electrospun polyimide nanofibers membrane," *Sci. Rep.*, vol. 10, no. 1, pp. 1–9, 2020, doi:

10.1038/s41598-020-59546-7.

[26] X. Peng *et al.*, "A breathable, biodegradable, antibacterial, and self-powered electronic skin based on all-nanofiber triboelectric nanogenerators," *Sci. Adv.*, vol. 6, no. 26, 2020, doi: 10.1126/sciadv.aba9624.

[27] B. Yu, H. Yu, T. Huang, H. Wang, and M. Zhu, "A biomimetic nanofiber-based triboelectric nanogenerator with an ultrahigh transfer charge density," *Nano Energy*, vol. 48, no. February, pp. 464–470, 2018, doi: 10.1016/j.nanoen.2018.03.064.

[28] T. Bhatta *et al.*, "High-performance triboelectric nanogenerator based on MXene functionalized polyvinylidene fluoride composite nanofibers," *Nano Energy*, vol. 81, no. December 2020, p. 105670, 2021, doi: 10.1016/j.nanoen.2020.105670.

[29] J. H. Zhang, Y. Li, J. Du, X. Hao, and H. Huang, "A high-power wearable triboelectric nanogenerator prepared from self-assembled electrospun poly(vinylidene fluoride) fibers with a heart-like structure," *J. Mater. Chem. A*, vol. 7, no. 19, pp. 11724–11733, 2019, doi: 10.1039/c9ta01956a.

[30] B. Dudem, D. H. Kim, A. R. Mule, and J. S. Yu, "Enhanced Performance of Microarchitectured PTFE-Based Triboelectric Nanogenerator via Simple Thermal Imprinting Lithography for Self-Powered Electronics," *ACS Appl. Mater. Interfaces*, vol. 10, no. 28, pp. 24181–24192, 2018, doi: 10.1021/acsami.8b06295.

[31] J. Yu *et al.*, "Flexible PDMS-based triboelectric nanogenerator for instantaneous force sensing and human joint movement monitoring," *Sci. China Mater.*, vol. 62, no. 10, pp. 1423–1432, 2019, doi: 10.1007/s40843-019-9446-1.

[32] X. Wang, B. Yang, J. Liu, Y. Zhu, C. Yang, and Q. He, "A flexible triboelectric-piezoelectric hybrid nanogenerator based on P(VDF-TrFE) nanofibers and PDMS/MWCNT for wearable devices," *Sci. Rep.*, vol. 6, no. October, pp. 1–10, 2016, doi: 10.1038/srep36409.

[33] Y. Wu, J. Qu, W. A. Daoud, L. Wang, and T. Qi, "Flexible composite-nanofiber based piezo-triboelectric nanogenerators for wearable electronics," *J. Mater. Chem. A*, vol. 7, no. 21, pp. 13347–13355, 2019, doi: 10.1039/c9ta02345c.

[34] C. Zhang, T. Zhou, W. Tang, C. Han, L. Zhang, and Z. L. Wang, "Rotating-disk-based direct-current triboelectric nanogenerator," *Adv. Energy Mater.*, vol. 4, no. 9, pp. 1–7, 2014, doi: 10.1002/aenm.201301798.

[35] H. J. Oh *et al.*, "A highly porous nonwoven thermoplastic polyurethane/polypropylene-based triboelectric nanogenerator for energy harvesting by human walking," *Polymers (Basel).*, vol. 12, no. 5, pp. 1–11, 2020, doi: 10.3390/POLYM12051044.

[36] A. Yar, A. Karabiber, A. Ozen, F. Ozel, and S. Coskun, "Flexible nanofiber based triboelectric nanogenerators with high power conversion," *Renew. Energy*, vol. 162, pp. 1428–1437, 2020, doi: 10.1016/j.renene.2020.08.030.

[37] S. Cui, Y. Zheng, J. Liang, and D. Wang, "Triboelectrification based on double-layered polyaniline nanofibers for self-powered cathodic protection driven by wind," *Nano Res.*, vol. 11, no. 4, pp. 1873–1882, 2018, doi: 10.1007/s12274-017-1805-y.

[38] S. R. Kim, J. H. Yoo, and J. W. Park, "Using Electrospun AgNW/P(VDF-TrFE) Composite Nanofibers to Create Transparent and Wearable Single-Electrode Triboelectric Nanogenerators for Self-Powered Touch Panels," *ACS Appl. Mater. Interfaces*, vol. 11, no. 16, pp. 15088–15096, 2019, doi: 10.1021/acsami.9b03338.

[39] G. Q. Gu *et al.*, "Triboelectric Nanogenerator Enhanced Nanofiber Air Filters for Efficient Particulate Matter Removal," *ACS Nano*, vol. 11, no. 6, pp. 6211–6217, 2017, doi: 10.1021/acsnano.7b02321.

[40] S. Wang *et al.*, "A facile respiration-driven triboelectric nanogenerator for multifunctional respiratory monitoring," *Nano Energy*, vol. 58, no. January, pp. 312–321, 2019, doi: 10.1016/j.nanoen.2019.01.042.

[41] M. H. Syu, Y. J. Guan, W. C. Lo, and Y. K. Fuh, "Biomimetic and porous nanofiber-based hybrid sensor for multifunctional pressure sensing and human gesture identification via deep learning method," *Nano Energy*, vol. 76, no. 300, p. 105029, 2020, doi: 10.1016/j.nanoen.2020.105029.

[42] X. Hu *et al.*, "Highly Sensitive P(VDF-TrFE)/BTO Nanofiber-Based Pressure Sensor with Dense Stress Concentration Microstructures," *ACS Appl. Polym. Mater.*, vol. 2, no. 11, pp. 4399–4404, 2020, doi: 10.1021/acsapm.0c00411.

[43] T. Huang, H. Yu, H. Wang, Q. Zhang, and M. Zhu, "Hydrophobic SiO2 Electret Enhances the Performance of Poly(vinylidene fluoride) Nanofiber-Based Triboelectric Nanogenerator," *J. Phys. Chem. C*, vol. 120, no. 47, pp. 26600–26608, 2016, doi: 10.1021/acs.jpcc.6b07382.

[44] G. Q. Gu *et al.*, "Triboelectric nanogenerator enhanced multilayered antibacterial nanofiber air filters for efficient removal of ultrafine particulate matter," *Nano Res.*, vol. 11, no. 8, pp. 4090–4101, 2018, doi: 10.1007/s12274-018-1992-1.

[45] H. Y. Mi *et al.*, "High-performance flexible triboelectric nanogenerator based on porous aerogels and electrospun nanofibers for energy harvesting and sensitive self-powered sensing," *Nano Energy*, vol. 48, no. February, pp. 327–336, 2018, doi: 10.1016/j.nanoen.2018.03.050.

[46] J. Liu, L. Zhang, N. Wang, and C. Li, "Highly stretchable and transparent triboelectric nanogenerator based on multilayer structured stable electrode for self-powered wearable sensor," *Nano Energy*, vol. 78, no. July, p. 105385, 2020, doi: 10.1016/j.nanoen.2020.105385.

[47] H. Y. Mi *et al.*, "High-performance flexible triboelectric nanogenerator based on porous aerogels and electrospun nanofibers for energy harvesting and sensitive self-powered sensing," *Nano Energy*, vol. 48. pp. 327–336, 2018, doi: 10.1016/j.nanoen.2018.03.050.

[48] S. Y. Hong *et al.*, "Stretchable Active Matrix Temperature Sensor Array of Polyaniline Nanofibers for Electronic Skin," *Adv. Mater.*, vol. 28, no. 5, pp. 930–935, 2016, doi: 10.1002/adma.201504659.

[49] C. C. Huang, Z. K. Kao, and Y. C. Liao, "Flexible miniaturized nickel oxide thermistor arrays via inkjet printing technology," *ACS Appl. Mater. Interfaces*, vol. 5, no. 24, pp.

12954–12959, 2013, doi: 10.1021/am404872j.

[50] H. Xu *et al.*, "Multifunctional Wearable Sensing Devices Based on Functionalized Graphene Films for Simultaneous Monitoring of Physiological Signals and Volatile Organic Compound Biomarkers," *ACS Appl. Mater. Interfaces*, vol. 10, no. 14, pp. 11785–11793, 2018, doi: 10.1021/acsami.8b00073.

[51] P. Huang *et al.*, "Textile-based triboelectric nanogenerators for wearable self-powered microsystems," *Micromachines*, vol. 12, no. 2, 2021, doi: 10.3390/mi12020158.

[52] Y. Khan *et al.*, "Flexible Hybrid Electronics: Direct Interfacing of Soft and Hard Electronics for Wearable Health Monitoring," *Adv. Funct. Mater.*, vol. 26, no. 47, pp. 8764–8775, 2016, doi: 10.1002/adfm.201603763.

[53] W. Paosangthong, R. Torah, and S. Beeby, "Recent progress on textile-based triboelectric nanogenerators," *Nano Energy*, vol. 55. pp. 401–423, 2019, doi: 10.1016/j.nanoen.2018.10.036.

[54] B. Shi *et al.*, "Body-Integrated Self-Powered System for Wearable and Implantable Applications," *ACS Nano*, vol. 13, no. 5. pp. 6017–6024, 2019, doi: 10.1021/acsnano.9b02233.

[55] Y. Guo *et al.*, "All-fiber hybrid piezoelectric-enhanced triboelectric nanogenerator for wearable gesture monitoring," *Nano Energy*, vol. 48. pp. 152–160, 2018, doi: 10.1016/j.nanoen.2018.03.033.

[56] Y. Cheng *et al.*, "A stretchable fiber nanogenerator for versatile mechanical energy harvesting and self-powered full-range personal healthcare monitoring," *Nano Energy*, vol. 41. pp. 511–518, 2017, doi: 10.1016/j.nanoen.2017.10.010.

[57] J. Xiong *et al.*, "Skin-touch-actuated textile-based triboelectric nanogenerator with black phosphorus for durable biomechanical energy harvesting," *Nature Communications*, vol. 9, no. 1. 2018, doi: 10.1038/s41467-018-06759-0.

[58] C. Jiang *et al.*, "All-electrospun flexible triboelectric nanogenerator based on metallic MXene nanosheets," *Nano Energy*, vol. 59. pp. 268–276, 2019, doi: 10.1016/j.nanoen.2019.02.052.

[59] T. Huang, M. Lu, H. Yu, Q. Zhang, H. Wang, and M. Zhu, "Enhanced power output of a triboelectric nanogenerator composed of electrospun nanofiber mats doped with graphene oxide," *Scientific Reports*, vol. 5. 2015, doi: 10.1038/srep13942.

[60] S. Cheon *et al.*, "High-Performance Triboelectric Nanogenerators Based on Electrospun Polyvinylidene Fluoride–Silver Nanowire Composite Nanofibers," *Advanced Functional Materials*, vol. 28, no. 2. 2018, doi: 10.1002/adfm.201703778.

[61] "Gas identification with graphene plasmons _ Enhanced Reader.pdf." .

[62] M. M. Alam, S. Lee, M. Kim, K. S. Han, V. A. Cao, and J. Nah, "Ultra-flexible nanofiber-based multifunctional motion sensor," *Nano Energy*, vol. 72, no. January, p. 104672, 2020, doi: 10.1016/j.nanoen.2020.104672.

[63] Z. Qin *et al.*, "Flexible Janus Electrospun Nanofiber Films for Wearable Triboelectric Nanogenerator," *Adv. Mater. Technol.*, vol. 5, no. 2, pp. 1–9, 2020, doi: 10.1002/admt.201900859.

[64] Z. Qin, Y. Yin, W. Zhang, C. Li, and K. Pan, "Wearable and Stretchable Triboelectric Nanogenerator Based on Crumpled Nanofibrous Membranes," *ACS Appl. Mater. Interfaces*, vol. 11, no. 13, pp. 12452–12459, 2019, doi: 10.1021/acsami.8b21487.

[65] K. Sarkar *et al.*, "Electrospinning to Forcespinning™," *Mater. Today*, vol. 13, no. 11, pp. 12–14, 2010, doi: 10.1016/S1369-7021(10)70199-1.

[66] S. S. H. Abir, S. K. Gupta, A. Ibrahim, B. B. Srivastava, and K. Lozano, "Tunable CsPb(Br/Cl) 3 perovskite nanocrystals and further advancement in designing light emitting fiber membranes," *Mater. Adv.*, vol. 2, pp. 2700–2710, 2021, doi: 10.1039/d1ma00183c.

[67] A. Sengupta, S. Das, S. Dasgupta, P. Sengupta, and P. Datta, "Flexible Nanogenerator from Electrospun PVDF − Polycarbazole Nano fi ber Membranes for Human Motion Energy-Harvesting Device Applications," 2021, doi: 10.1021/acsbiomaterials.0c01730.

[68] R. Vasita and D. S. Katti, "Nanofibers and their applications in tissue engineering," *Int. J. Nanomedicine*, vol. 1, no. 1, pp. 15–30, 2006, doi: 10.2147/nano.2006.1.1.15.

[69] K. Ulubayram, S. Calamak, R. Shahbazi, and I. Eroglu, "Nanofibers Based Antibacterial Drug Design, Delivery and Applications," *Curr. Pharm. Des.*, vol. 21, no. 15, pp. 1930–1943, 2015, doi: 10.2174/1381612821666150302151804.

[70] I. S. Kurtz and J. D. Schiffman, "Current and emerging approaches to engineer antibacterial and antifouling electrospun nanofibers," *Materials (Basel).*, vol. 11, no. 7, 2018, doi: 10.3390/ma11071059.

[71] S. Sundarrajan, K. L. Tan, S. H. Lim, and S. Ramakrishna, "Electrospun nanofibers for air filtration applications," *Procedia Eng.*, vol. 75, pp. 159–163, 2014, doi: 10.1016/j.proeng.2013.11.034.

[72] P. Zhou *et al.*, "Synthesis and Electrochemical Performance of ZnSe Electrospinning Nanofibers as an Anode Material for Lithium Ion and Sodium Ion Batteries," *Frontiers in Chemistry*, vol. 7. 2019, doi: 10.3389/fchem.2019.00569.

[73] M. A. Sobhan, A. Lebedev, L. L. Chng, and F. Anariba, "Rapid fabrication of photoluminescent electrospun nanofibers without the need of chemical polymeric backbone modifications," *J. Nanomater.*, vol. 2018, 2018, doi: 10.1155/2018/1980357.

[74] L. Zhang *et al.*, "Enhanced performance of piezoelectric nanogenerator based on aligned nanofibers and three-dimensional interdigital electrodes," *Nano Energy*, vol. 65, no. August, p. 103924, 2019, doi: 10.1016/j.nanoen.2019.103924.

[75] Y. Li, M. A. Abedalwafa, L. Tang, D. Li, and L. Wang, *Electrospun nanofibers for sensors*. 2018.

[76] I. Alghoraibi and S. Alomari, "Different Methods for Nanofiber Design and Fabrication," in *Handbook of Nanofibers*, A. Barhoum, M. Bechelany, and A. Makhlouf, Eds. Cham:

Springer International Publishing, 2018, pp. 1–46.

[77] X. Pu, J. W. Zha, C. L. Zhao, S. B. Gong, J. F. Gao, and R. K. Y. Li, "Flexible PVDF/nylon-11 electrospun fibrous membranes with aligned ZnO nanowires as potential triboelectric nanogenerators," *Chem. Eng. J.*, vol. 398, no. 30, p. 125526, 2020, doi: 10.1016/j.cej.2020.125526.

[78] H. Zou *et al.*, "Quantifying the triboelectric series," *Nat. Commun.*, vol. 10, no. 1, pp. 1–9, 2019, doi: 10.1038/s41467-019-09461-x.

[79] Q. Jing and S. Kar-Narayan, "Nanostructured polymer-based piezoelectric and triboelectric materials and devices for energy harvesting applications," *J. Phys. D. Appl. Phys.*, vol. 51, no. 30, 2018, doi: 10.1088/1361-6463/aac827.

[80] G. I. Dzhardimalieva, B. C. Yadav, T. V. Lifintseva, and I. E. Uflyand, "Polymer chemistry underpinning materials for triboelectric nanogenerators (TENGs): Recent trends," *Eur. Polym. J.*, vol. 142, no. August 2020, p. 110163, 2021, doi: 10.1016/j.eurpolymj.2020.110163.

[81] W. Yang, Y. Li, L. Feng, Y. Hou, S. Wang, and B. Yang, "GO / Bi 2 S 3 Doped PVDF / TPU Nanofiber Membrane with Enhanced Photothermal Performance."

[82] W. Wu *et al.*, "Enhanced MPBR with polyvinylpyrrolidone-graphene oxide/PVDF hollow fiber membrane for efficient ammonia nitrogen wastewater treatment and high-density Chlorella cultivation," *Chem. Eng. J.*, vol. 379, no. July 2019, p. 122368, 2020, doi: 10.1016/j.cej.2019.122368.

[83] S. Lanceros-Méndez, J. F. Mano, A. M. Costa, and V. H. Schmidt, "FTIR and DSC studies of mechanically deformed β-PVDF films," *J. Macromol. Sci. - Phys.*, vol. 40 B, no. 3–4, pp. 517–527, 2001, doi: 10.1081/MB-100106174.

[84] A. Asefnejad, M. T. Khorasani, A. Behnamghader, B. Farsadzadeh, and S. Bonakdar, "Manufacturing of biodegradable polyurethane scaffolds based on polycaprolactone using a phase separation method: physical properties and in vitro assay.," *Int. J. Nanomedicine*, vol. 6, no. October 2011, pp. 2375–2384, 2011, doi: 10.2147/ijn.s15586.

[85] J. W. Li, H. T. Lee, H. A. Tsai, M. C. Suen, and C. W. Chiu, "Synthesis and properties of novel polyurethanes containing long-segment fluorinated chain extenders," *Polymers (Basel).*, vol. 10, no. 11, 2018, doi: 10.3390/POLYM10111292.

[86] E. Fallahiarezoudar, M. Ahmadipourroudposht, A. Idris, and N. M. Yusof, "Optimization and development of Maghemite (γ-Fe2O3) filled poly-L-lactic acid (PLLA)/thermoplastic polyurethane (TPU) electrospun nanofibers using Taguchi orthogonal array for tissue engineering heart valve," *Mater. Sci. Eng. C*, vol. 76, pp. 616–627, 2017, doi: 10.1016/j.msec.2017.03.120.

[87] A. M. Abdullah, A. Flores, A. R. Chowdhury, J. Li, Y. Mao, and M. J. Uddin, "Synthesis and fabrication of self-sustainable triboelectric energy case for powering smart electronic devices," *Nano Energy*, vol. 73, no. February, p. 104774, 2020, doi: 10.1016/j.nanoen.2020.104774.

[88] A. R. Chowdhury *et al.*, "Lithium doped zinc oxide based flexible piezoelectric-triboelectric

hybrid nanogenerator," *Nano Energy*, vol. 61, no. February, pp. 327–336, 2019, doi: 10.1016/j.nanoen.2019.04.085.

[89] X. He *et al.*, "A Hierarchically Nanostructured Cellulose Fiber-Based Triboelectric Nanogenerator for Self-Powered Healthcare Products," *Advanced Functional Materials*, vol. 28, no. 45. 2018, doi: 10.1002/adfm.201805540.

[90] S. Parandeh, M. Kharaziha, and F. Karimzadeh, "An eco-friendly triboelectric hybrid nanogenerators based on graphene oxide incorporated polycaprolactone fibers and cellulose paper," *Nano Energy*, vol. 59, no. December 2018, pp. 412–421, 2019, doi: 10.1016/j.nanoen.2019.02.058.

[91] M. F. Lin, J. Xiong, J. Wang, K. Parida, and P. S. Lee, "Core-shell nanofiber mats for tactile pressure sensor and nanogenerator applications," *Nano Energy*, vol. 44, no. November 2017, pp. 248–255, 2018, doi: 10.1016/j.nanoen.2017.12.004.

[92] Y. Zhou, W. Deng, J. Xu, and J. Chen, "Engineering Materials at the Nanoscale for Triboelectric Nanogenerators," *Cell Reports Phys. Sci.*, vol. 1, no. 8, p. 100142, 2020, doi: 10.1016/j.xcrp.2020.100142.

[93] Q. Ye *et al.*, "Effects of liquid metal particles on performance of triboelectric nanogenerator with electrospun polyacrylonitrile fiber films," *Nano Energy*, vol. 61, no. April, pp. 381–388, 2019, doi: 10.1016/j.nanoen.2019.04.075.

[94] G. Zhu, P. Bai, J. Chen, and Z. Lin Wang, "Power-generating shoe insole based on triboelectric nanogenerators for self-powered consumer electronics," *Nano Energy*, vol. 2, no. 5, pp. 688–692, 2013, doi: 10.1016/j.nanoen.2013.08.002.

[95] X. Pu *et al.*, "Ultrastretchable, transparent triboelectric nanogenerator as electronic skin for biomechanical energy harvesting and tactile sensing," *Sci. Adv.*, vol. 3, no. 5, pp. 1–11, 2017, doi: 10.1126/sciadv.1700015.

BIOGRAPHICAL SKETCH

Sk Shamim Hasan Abir was born in a small city of Bangladesh named Jessore. He completed his elementary and high school from Jessore then moved to the capital city of Bangladesh, Dhaka. There he completed his bachelor's degree in mechanical engineering where he received DEANS award for three consecutive years and Board scholarship for four years for his outstanding results in higher secondary.

After completing his undergraduate he moved to USA to pursue his master's degree. He joined University of Texas Rio Grande Valley (UTRGV) to do his master's in mechanical engineering. During his MS, he worked as Research assistant under Dr. Karen Lozano and Teaching assistant under Dr. Dumitru Caruntu. He worked on multiple projects included polymer nanocomposite, synthesis of perovskite nanocrystals, photoluminescent nanofiber and nanofiber based triboelectric nanogenerator. He received Presidential Graduate Research Assistantship for his performance for two years during his study at UTRGV.

He was awarded a Master of Science in Engineering in Mechanical Engineering, from the University of Texas Rio Grande Valley in August of 2021. and wished to join in Texas A&M university for his PhD study in material science and engineering. His research interests are fabrication of polymer nanocomposite based medical device and sensor and semiconductor material for flexible energy storage device. He can be reached through his personal email address at any time shamimhasanabir@gmail.com.